

## A novel potent oral series of VEGFR2 inhibitors abrogate tumor growth by inhibiting angiogenesis.

Guido Bold, Christian Schnell, Pascal Furet, Paul McSheehy, Josef Brügger, Mestan Jürgen, Paul William Manley, Peter Druce, Marion Burglin, Ursula Dürler, Jacqueline Loretan, Robert Reuter, Markus Wartmann, Andreas Theuer, Beatrice Bauer-Probst, Georg Martiny-Baron, Peter Allegrini, Arnaud Goepfert, Jeanette Wood, and Amanda Littlewood-Evans

*J. Med. Chem.*, **Just Accepted Manuscript** • DOI: 10.1021/acs.jmedchem.5b01582 • Publication Date (Web): 02 Dec 2015

Downloaded from <http://pubs.acs.org> on December 4, 2015

### Just Accepted

“Just Accepted” manuscripts have been peer-reviewed and accepted for publication. They are posted online prior to technical editing, formatting for publication and author proofing. The American Chemical Society provides “Just Accepted” as a free service to the research community to expedite the dissemination of scientific material as soon as possible after acceptance. “Just Accepted” manuscripts appear in full in PDF format accompanied by an HTML abstract. “Just Accepted” manuscripts have been fully peer reviewed, but should not be considered the official version of record. They are accessible to all readers and citable by the Digital Object Identifier (DOI®). “Just Accepted” is an optional service offered to authors. Therefore, the “Just Accepted” Web site may not include all articles that will be published in the journal. After a manuscript is technically edited and formatted, it will be removed from the “Just Accepted” Web site and published as an ASAP article. Note that technical editing may introduce minor changes to the manuscript text and/or graphics which could affect content, and all legal disclaimers and ethical guidelines that apply to the journal pertain. ACS cannot be held responsible for errors or consequences arising from the use of information contained in these “Just Accepted” manuscripts.

1

**A novel potent oral series of VEGFR2 inhibitors abrogate tumor growth by inhibiting angiogenesis.**

**Guido Bold\***, Christian Schnell, Pascal Furet, Paul McSheehy, Josef Brügggen, Jürgen Mestan, Paul W. Manley, Peter Drückes, Marion Burglin, Ursula Dürler, Jacqueline Loretan, Robert Reuter, Markus Wartmann, Andreas Theuer, Beatrice Bauer-Probst, Georg Martiny-Baron, Peter Allegrini, Arnaud Goepfert, Jeanette Wood and Amanda Littlewood-Evans\*

*Novartis Institutes for BioMedical Research, Oncology Research, 4002 Basel, Switzerland.*

**Abstract****Keywords VEGFR2, Inhibitor, tumor angiogenesis, BAW2881, BFH772**

This paper describes the identification of 6-(pyrimidin-4-yloxy)-naphthalene-1-carboxamides as a new class of potent and selective human vascular endothelial growth factor receptor 2 (VEGFR2) tyrosine kinase inhibitors.

In biochemical and cellular assays the compounds exhibit single digit nanomolar potency towards VEGFR2.

Compounds of this series show good exposure in rodents when dosed orally. They potently inhibit VEGF-driven angiogenesis in a chamber model and rodent tumor models at daily doses of less than 3 mg/kg by targeting the tumor vasculature as demonstrated by ELISA for TIE-2 in lysates, or by immunohistochemical analysis. This novel series of compounds shows a potential for the treatment of solid tumors and other diseases where angiogenesis plays an important role.

**Introduction**

Angiogenesis is the formation of new vessels from existing ones, whereas vasculogenesis is the formation of new vessels from hematopoietic precursors. Both processes are reliant upon vascular endothelial growth factor (VEGF) and its family of receptors (VEGFR).<sup>1</sup> The VEGF family, which includes VEGF-A, VEGF-B, VEGF-C, VEGF-D and placental growth factor (PlGF), signals via VEGFR2, VEGFR1 and VEGFR3 cell surface tyrosine kinase receptors located on the host vascular endothelium, lymphatic and hematopoietic system.<sup>2</sup> These receptors become autophosphorylated at the tyrosine kinase domain upon engagement of VEGF which subsequently leads to downstream events resulting in proliferation and migration of the vasculature.

2

1  
2  
3 Although these are normal processes in wound healing and during the female reproductive cycle, aberrant  
4  
5 angiogenesis and vasculogenesis are observed in a number of pathological conditions such as rheumatoid  
6  
7 arthritis, psoriasis, retinal complications and tumor growth.<sup>3</sup>  
8  
9

10  
11 Growth of most solid tumors is highly dependent on the presence of newly formed vessels which provide  
12  
13 nutrients and oxygen to the tumor microenvironment.<sup>4</sup> VEGF has been shown to be secreted by tumor cells  
14  
15 thereby encouraging new growth and maintenance of a vascular network and culminating in promotion of  
16  
17 metastatic spread.<sup>5</sup>  
18  
19

20  
21 Since the main pro-angiogenic signal for vasculature stems from VEGFR2 (also known as KDR), specific  
22  
23 inhibition of signal transduction via the VEGF / VEGFR system is a promising approach to starve the tumor  
24  
25 cells of nutrients and thus impede tumor growth<sup>6</sup> and metastasis.<sup>7</sup>  
26  
27

28  
29 The respective biology and progress in modulating this system have been summarized in recent review articles.<sup>8</sup>  
30

31 In a collaborative effort between CIBA/Novartis and Schering AG, the phthalazine Vatalanib (PTK787 /  
32  
33 ZK222584)<sup>9</sup>, and the anthranilamide AAL993<sup>10</sup> have been discovered as potent and selective VEGFR2  
34  
35 inhibitors (see Fig. 1). In a new screen for follow up compounds, the observation that the FLT3 inhibitor  
36  
37 AST487 also inhibits VEGFR2 autophosphorylation (see Fig. 1) resulted in the discovery of the 6-(pyrimidin-4-  
38  
39 yloxy)-naphthalene-1-carboxamides, as a new class of potent and selective VEGFR inhibitors. The activity but  
40  
41 not the structure of two of the compounds within this series, BFH772 and BAW2881, have been described  
42  
43 previously.<sup>11</sup> Herein we describe their structure, synthesis and *in vitro* potency, which translates to excellent *in*  
44  
45 *vivo* activities. We compare their profile to our forerunner compounds PTK787 and AAL993 as well as  
46  
47 evaluating them against established kinase inhibitors, in particular Sorafenib (Bayer/Onyx pharmaceuticals) and  
48  
49 Sunitinib (Pfizer).  
50  
51  
52  
53  
54  
55  
56  
57  
58  
59  
60

3

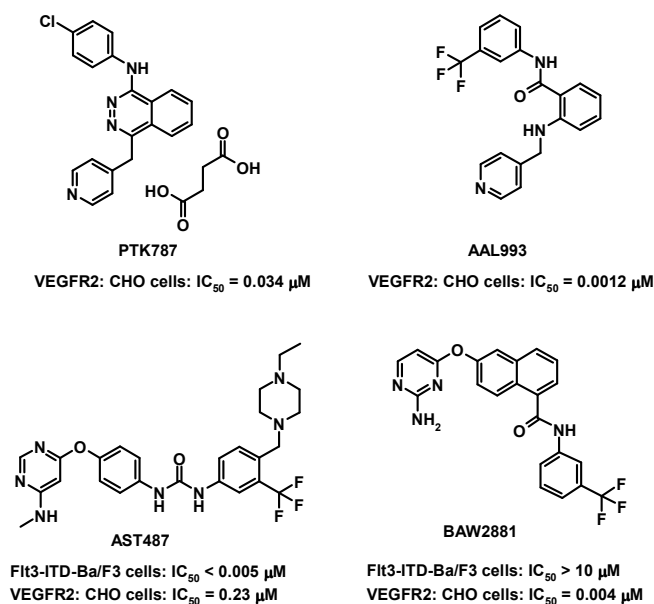


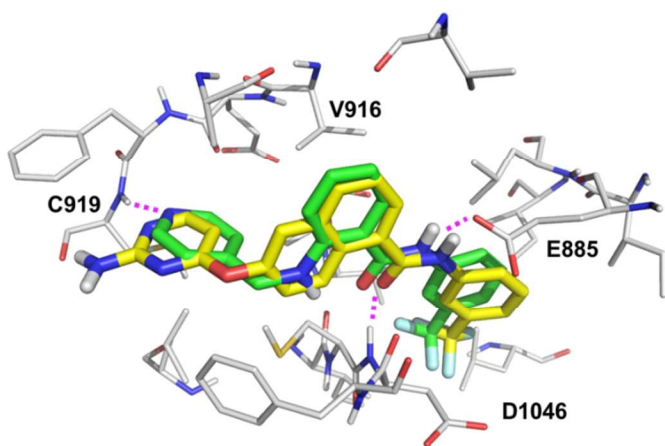
**Figure 1:** Forerunner compounds PTK787 and AAL993 are shown in comparison to AST487 and later generation BAW2881. Comparative inhibitory activity towards VEGFR2 versus FLT3 in cellular assays shown for the latter two compounds.

## Chemistry

The kinase inhibitor AST487 was originally designed as an FLT3 inhibitor. It was synthesized as described by Shieh *et al.*<sup>12</sup> In the FLT3-ITD-Ba/F3 cell system AST487 blocked FLT3 dependent cell proliferation with an  $IC_{50}$  value  $< 5 \text{ nM}$ .<sup>13</sup> However, it exhibited only moderate selectivity for FLT3.<sup>14</sup> Besides its effects on RET kinase, AST487 also inhibited VEGFR2, VEGFR3, KIT, and ABL. Of special interest was its inhibitory activity against VEGFR2; with the compound demonstrating an  $IC_{50}$  value of  $0.23 \mu\text{M}$  in a VEGF-driven cellular receptor autophosphorylation assay in CHO cells transfected with the VEGFR2 receptor<sup>15</sup> (see Fig. 1). To understand its binding interactions with VEGFR2, we used the crystal structure of AAL993 in complex with the kinase domain of VEGFR2.<sup>16</sup> AAL993 binds to the inactive “DFG out” conformation of the VEGFR2 kinase as represented in Fig. 2. In addition to hydrogen bonds formed with residues C919, E885 and D1046, the inhibitor

4

1  
2 makes a key hydrophobic interaction with residue V916, the “gate keeper” residue. Analogous docking of  
3  
4  
5 AST487 into the binding pocket of AAL993 placed the aminopyrimidine residue as the hinge binding motif of  
6  
7 the inhibitor. Molecular modeling experiments indicated that replacing the anthranilic acid core of AAL993 by  
8  
9 a naphthyl moiety maintains all the favorable interactions of the inhibitor with the binding pocket. This design  
10  
11 concept illustrated in Fig. 2 led to the synthesis of BAW2881<sup>11</sup> in which the pyridine hinge binding moiety of  
12  
13 AAL993 was changed to an aminopyrimidine, as is the case for AST487. In contrast to AST487, BAW2881  
14  
15 showed higher potency and selectivity for VEGFR2 versus FLT3. The VEGF-driven cellular receptor  
16  
17 autophosphorylation in CHO cells of BAW2881 was inhibited with an IC<sub>50</sub> of 4 nM, in the same range as for  
18  
19 AAL993 and significantly more potent than for PKT787 (see Fig. 1).  
20  
21  
22  
23  
24  
25  
26  
27

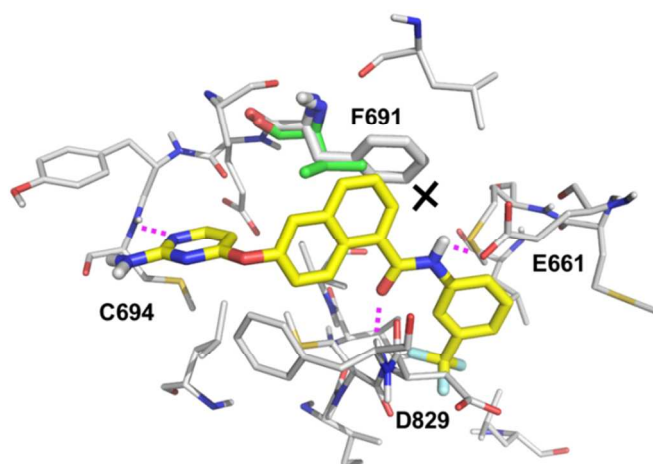


28  
29  
30  
31  
32  
33  
34  
35  
36  
37  
38  
39  
40  
41  
42  
43  
44 **Figure 2:** AAL993 (green) bound in the ATP pocket of the  
45 VEGFR2 kinase (PDB code 5EW3).<sup>16</sup> Only the residues  
46 proximal to the inhibitor are represented. Hydrogen bonds  
47 appear as dashed lines. BAW2881 docked in the pocket  
48 according to the design concept (yellow).  
49  
50  
51  
52  
53  
54  
55  
56  
57

58 Docking of BAW2881 in a homology model of the kinase domain of FLT3 in the “DFG out” conformation<sup>17</sup>  
59 provided a hypothesis to explain the lack of FLT3 inhibitory activity of this compound. As shown in Fig. 3,  
60

5

1  
2 BAW2881 can form interactions with FLT3 similar to those formed with VEGFR2. However, the “gate keeper”  
3  
4 residue in FLT3 is a phenylalanine (F691). It is bulkier than in VEGFR2 which has a valine (V916) instead. As  
5  
6 a consequence, there is not enough space in the FLT3 ATP binding site to accommodate the upper phenyl ring  
7  
8 of the naphthyl core of BAW2881. Thus, the docking model suggested a steric clash between this phenyl ring  
9  
10 and F691 explaining the lack of FLT3 inhibitory activity of BAW2881.  
11  
12  
13  
14  
15  
16  
17  
18  
19  
20  
21  
22  
23  
24  
25  
26  
27  
28  
29  
30  
31  
32  
33  
34



35 **Figure 3:** BAW2881 docked in the ATP binding site of a  
36  
37 homology model of the kinase domain of FLT3 in the “DFG  
38  
39 out” conformation (constructed based on PDB structure  
40  
41 1UWH). The steric clash between the “gate keeper” residue  
42  
43 F691 and the naphthyl core of the compound is indicated by a  
44  
45 cross. The smaller valine “gate keeper” residue of VEGFR2 is  
46  
47 shown in green.  
48  
49  
50  
51  
52  
53  
54  
55

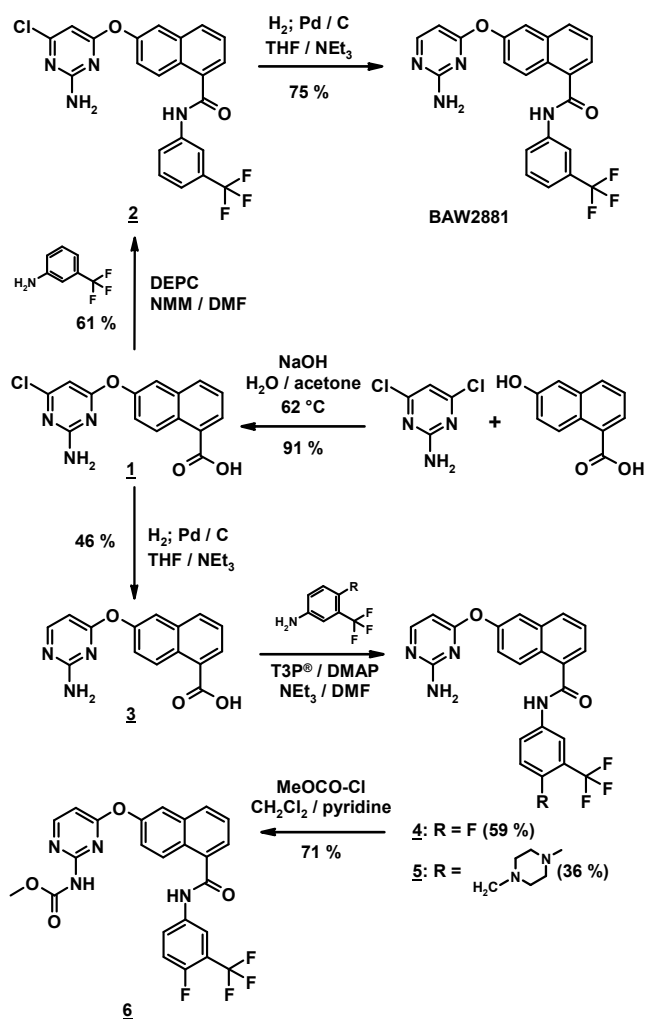
56 The synthesis of the 6-(2-amino-pyrimidin-4-yloxy)-naphthalene-1-carboxamides is described in Scheme 1:

57  
58 Diarylether formation from 2-amino-4,6-dichloro-pyrimidine and 6-hydroxy-naphthyl carboxylate resulted in **1**.  
59  
60

6

Amide formation with 3-trifluoromethylaniline with DEPC as the coupling reagent ( $\rightarrow$  **2**), followed by hydrogenative dechlorination led to BAW2881. Alternatively, dechlorination of **1** gave the acid **3**, which then could be converted by T3P<sup>®</sup> (*N*-propylphosphonic acid anhydride, cyclic trimer) to the amides **4** and **5**.

Acylation of **4** with methyl chloroformate gave **6**.

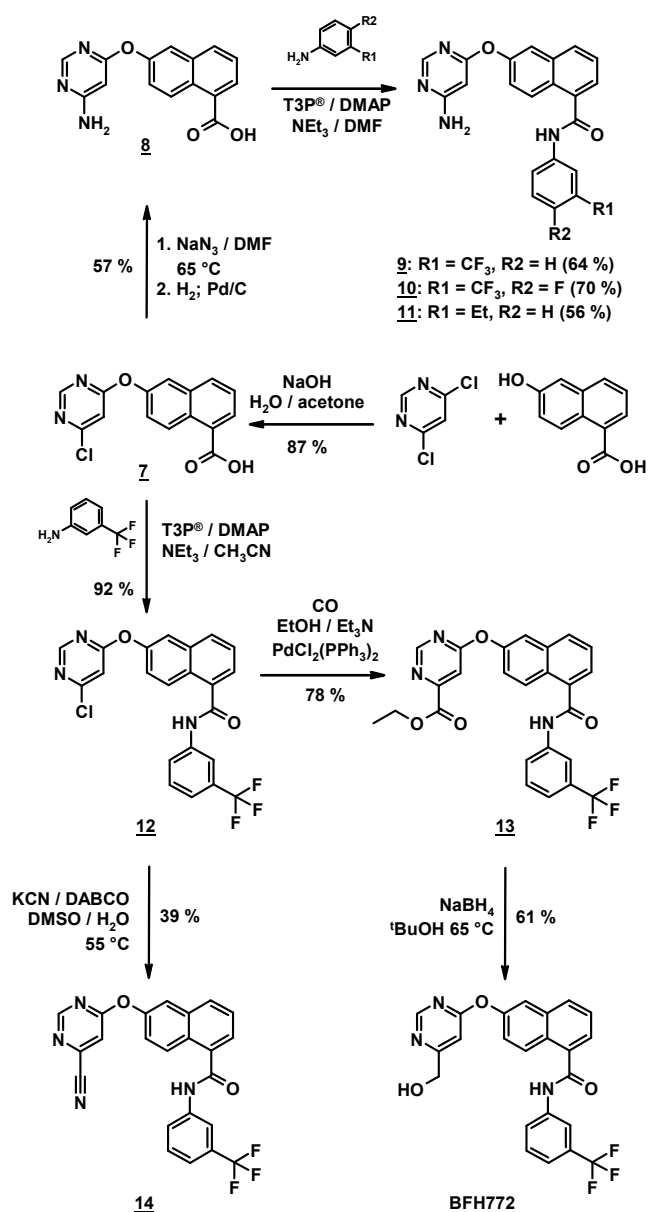


**Scheme 1:** Synthesis of the 6-(2-amino-pyrimidin-4-yloxy)-naphthalene-1-carboxylic acid amides BAW2881, **4**, **5** and **6**.

Etherification of 4,6-dichloro-pyrimidine resulted in **7** (see Scheme 2). Substitution of the chlorine by azide and reduction led to 6-(6-amino-pyrimidin-4-yloxy)-naphthalene carboxylate (**8**), which then was transformed into the amides **9-11**. Amide formation on **7** yielded the 6-(6-chloro-pyrimidin-4-yloxy)-naphthalene carboxamide

7

12. Carbonylation in ethanol employing Pd-catalysis then provided the ethylester **13**, which was reduced by NaBH<sub>4</sub> in *t*-butanol to the hydroxymethyl derivative BFH772. Replacement of the chlorine in **12** by cyanide gave the nitrile **14**.



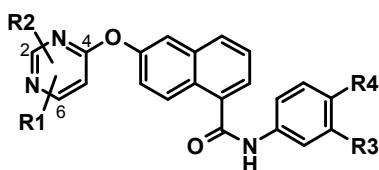
54 **Scheme 2:** Synthesis of the 6-(pyrimidin-4-yloxy)-  
 55 naphthalene-1-carboxylic acid amides **9-11**, **13**, BFH772 and  
 56  
 57  
 58 **14**.

8

**Biology****SAR around the 6-(pyrimidin-4-yloxy)-naphthalene-1-carboxylic acid phenylamide structure type series**

Table 1 summarizes the SAR around the 6-(pyrimidin-4-yloxy)-naphthalene-1-carboxylic acid phenylamide structure type series in respect of its inhibitory potency against VEGFR2. Potency was assessed using a biochemical assay for VEGFR inhibition and a cellular test system addressing CHO autophosphorylation described in detail by Wood *et al.*<sup>15</sup> An additional substituent at position 6 of the pyrimidine (2-amino-6-chloro-pyrimidine derivative **2**) was not tolerated consistent with the binding model (Fig. 2) indicating a steric clash of the chlorine atom with the kinase hinge region. Moving the amino substituent to the 6-position of the pyrimidine led to **9**, which exhibited similar activity compared to BAW2881. This was expected due to the ability of aminopyrimidine groups to form bidentate hydrogen bonds with the hinge segment centered around C919. A 6-cyano derivative (**14**) was a slightly weaker inhibitor. Even less active was the 6-ethoxy-carbonyl derivative **13** which, according to the model, was also clashing in the hinge region. In contrast a 6-hydroxymethyl substituent on the pyrimidine (BFH772) led to a potent derivative. In the aniline part, a blocking fluorine at the 4-position of the phenyl ring was well tolerated (**4**, **10**). Replacing the 3-trifluoromethyl group by ethyl led to the highly active derivative **11**. Expanding the 4-position of the anilide with a piperazinyl-methyl group (**5**), as is the case for AST487, retained kinase activity but decreased the cellular potency for VEGFR2. Compound **5** was less selective (data not shown) targeting other kinases more potently than BAW2881. Based on the binding model, the piperazinyl group was expected to establish bifurcated H-bonds with the backbone carbonyl groups of VEGFR2 residues Ile1025 and His1026. These interactions have been observed in several crystal structures of inhibitors binding to the “DFG out” conformation of kinases. The loss of selectivity observed with this modification is consistent with the conserved nature of backbone interactions. The decrease in VEGFR2 cellular potency despite the formation of new favorable interactions may thus be ascribed to a detrimental effect of the piperazinyl group on compound cell permeability. Acylation of the 2-amino-pyrimidine group was tolerated with regard to VEGFR2 inhibition (**6**).

9



cpd	R1	R2	R3	R4	Inhibition of VEGFR2 transphosphorylation (biochemical) ( $\mu\text{M}$ )	Inhibition of VEGFR2 autophosphorylation (CHO cells) ( $\mu\text{M}$ )
AST487					$0.003 \pm 0.001$	$0.23 \pm 0.06$
BAW2881	2-NH <sub>2</sub>		CF <sub>3</sub>		$0.009 \pm 0.003$	$0.0042 \pm 0.0002$
<u>2</u>	2-NH <sub>2</sub>	6-Cl	CF <sub>3</sub>		$1.18 \pm 0.21$	$0.4^a$
<u>9</u>	6-NH <sub>2</sub>		CF <sub>3</sub>		$0.004 \pm 0.0002$	$0.002 \pm 0.001$
<u>14</u>	6-CN		CF <sub>3</sub>		$0.037 \pm 0.003$	$0.021 \pm 0.005$
<u>13</u>	6-COOEt		CF <sub>3</sub>		$0.34 \pm 0.14$	$2.0^a$
BFH772	6-CH <sub>2</sub> OH		CF <sub>3</sub>		$0.0027 \pm 0.0009$	$0.0046 \pm 0.0006$
<u>4</u>	2-NH <sub>2</sub>		CF <sub>3</sub>	F	$0.007 \pm 0.001$	$0.004 \pm 0.001$
<u>10</u>	6-NH <sub>2</sub>		CF <sub>3</sub>	F	$0.006 \pm 0.002$	$0.003 \pm 0.001$
<u>11</u>	6-NH <sub>2</sub>		Et		$0.001 \pm 0.0003$	$0.001 \pm 0.0002$
<u>5</u>	2-NH <sub>2</sub>		CF <sub>3</sub>		$0.006 \pm 0.003$	$0.05^a$
<u>6</u>	2-NHCOOMe		CF <sub>3</sub>	F	$0.025 \pm 0.010$	$0.004 \pm 0.001$

**Table 1: SAR of 6-(pyrimidin-4-yloxy)-naphthalene-1-carboxamides in respect to VEGFR2 inhibition - Mean IC<sub>50</sub> values in  $\mu\text{M}$**

$\pm$  SEM are shown; <sup>a</sup> single experiment

10

### Biochemical IC<sub>50</sub> data on VEGFR family kinase activity

In our biochemical assay, the naphthalene-1-carboxamide series generated potent IC<sub>50</sub>s for VEGFR2 which were slightly more potent than the earlier generation compounds PTK787 and AAL993. The multi-kinase inhibitor Sunitinib from Pfizer and Bayer and Onyx's VEGFR, PDGFR and RAF compound Sorafenib were of equal potency in the hVEGFR2 kinase assay. BAW2881, **4**, **9** and **10** all lost potency (17-, 46-, 9- and 21-fold respectively) against murine enzyme (FLK-1) compared to hVEGFR2. In addition, they also lost potency towards human VEGFR1 (FLT-1) and human VEGFR3 (FLT-4) versus hVEGFR2. BFH772 was highly effective at targeting VEGFR2 kinase with an IC<sub>50</sub> value of 3 nM, however lost 500-fold potency on FLK-1, FLT-1 and FLT-4 (Table 2).

Kinase	BAW2881	BFH772	<u>4</u>	<u>9</u>	<u>10</u>	PTK787	AAL993	Sorafenib	Sunitinib
IC <sub>50</sub> (μM)									
hVEGFR2 (KDR)	0.009 ± 0.0037	0.0027 ± 0.0009	0.007 ± 0.001	0.004 ± 0.0002	0.006 ± 0.002	0.055 ± 0.001	0.023 ± 0.006	0.0078 ± 0.0009	0.0102 ± 0.0019
mVEGFR2 (FLK-1)	0.165 ± 0.064	1.5 ± 0.53	0.320 ± 0.097	0.037 ± 0.003	0.125 ± 0.026	0.27 ± 0.04	0.055 ± 0.013	nd	0.073 ± 0.008
hVEGFR1 (FLT-1)	0.82 ± 0.19	1.7 ± 0.36	0.223 ± 0.077	0.081 ± 0.002	0.333 ± 0.109	0.077 ± 0.012	0.13 ± 0.081	0.402 ± 0.146	0.015 ± 0.009
hVEGFR3 (FLT-4)	0.42 ± 0.015	1.1 ± 0.29	0.177 ± 0.052	0.050 ± 0.006	0.235 ± 0.043	0.064 ± 0.02	0.018 ± 0.001	0.245 ± 0.08	0.024 ± 0.0038

**Table 2: Inhibition of VEGFR family kinases** - Mean IC<sub>50</sub> values in μM ± SEM are shown. Kinase activity was tested by measuring the phosphorylation of a synthetic substrate (poly[Glu, Tyr]), by purified GST-fusion kinase domains of receptor tyrosine kinases, in the presence of radiolabelled ATP; ATP-concentrations used were optimized within the Km range for the individual kinases. nd is not determined.

11

## Selectivity – biochemical IC<sub>50</sub> data on other kinases

Overall the naphthalene-1-carboxamide series displayed similar selectivity to the forerunner compounds PTK787 and AAL993. BAW2881 inhibited a limited number of kinases including c-RAF, B-RAF, RET, ABL and TIE-2 at sub- $\mu\text{M}$  IC<sub>50</sub>s. BFH772 was highly selective; apart from inhibiting VEGFR2 at 3 nM IC<sub>50</sub>, it also targeted B-RAF, RET and TIE-2, albeit with at least 40-fold lower potency. These two compounds were inactive (IC<sub>50</sub> > 10  $\mu\text{M}$ ; > 2  $\mu\text{M}$  for cKIT) against all other tyrosine specific- and serine/threonine-specific protein kinases tested. Compounds **4**, **9** and **10** were also relatively specific but in addition to the aforementioned kinases, also showed activity against a number of other protein kinases including cKIT, and weakly against c-FMS. Sorafenib and Sunitinib displayed a broader spectrum of activity; with additional IC<sub>50</sub> values generated for FLT3, c-SRC, cMET, EphB4, CDK1 and FGFR3 (Supplementary Fig. 1).

## Cellular VEGFR2 assays

In cellular VEGF-induced VEGFR2 autophosphorylation assays, PTK787 was previously reported to have an IC<sub>50</sub> of  $17 \pm 2$  nM and  $34 \pm 2$  nM in HUVEC and CHO cells respectively<sup>9,15</sup> whereas AAL993 was more potent at  $1.2 \pm 0.19$  nM in the latter assay.<sup>10</sup> Sunitinib and Sorafenib, gave IC<sub>50</sub> values of  $8.75 \pm 0.75$  nM and  $8 \pm 0.5$  nM respectively when profiled in our VEGFR2 autophosphorylation assay in CHO cells. The VEGFR2 inhibitors of the 6-(pyrimidin-4-yloxy)-naphthalene-1-carboxamide structure class as exemplified by BAW2881, BFH772, **4**, **9** and **10** revealed 5- to 15-fold enhanced potency when compared to PTK787. They were in the same range as AAL993, Sorafenib and Sunitinib, exhibiting single digit nanomolar potency in the CHO cellular assay (Table 3).

12

IC <sub>50</sub> (μM)	BAW2881	BFH772	<u>4</u>	<u>9</u>	<u>10</u>	PTK787	AAL993
VEGFR2 (CHO)	0.0042 ± 0.0002	0.0046 ± 0.0006	0.004 ± 0.001	0.002 ± 0.001	0.003 ± 0.001	0.034 ± 0.002	0.0012 ± 0.0002
VEGFR2 (HUVEC)	0.0029 ± 0.0003	0.003 ± 0	0.004	0.003	0.0023	0.017 ± 0.002	nd

**Table 3: Inhibition of CHO and HUVEC VEGFR2 phosphorylation assays** – Mean IC<sub>50</sub> values (μM) for inhibition of KDR tyrosine kinase in CHO-VEGFR2 and HUVEC cells. nd is not determined.

### Cellular selectivity assays

#### RTK phosphorylation assays

BFH772 and BAW2881 were tested in an ELISA based assay measuring phosphorylation of the receptor tyrosine kinase after cells were stimulated with the respective ligand.

BFH772 and BAW2881 both inhibited the ligand induced autophosphorylation of RET, PDGFR and KIT kinases with IC<sub>50</sub> values ranging between 30 and 160 nM. The compounds were selective (IC<sub>50</sub> values > 0.5 μM) against the kinases of EGFR, ERBB2, INS-R and IGF-1R and against the cytoplasmic BCR-ABL kinase (Supplementary Fig. 2).

#### BaF3 cellular assays

The potential for compounds to inhibit various kinases in a cellular context was also determined in the Ba/F3 assay system consisting of wild-type IL-3-dependent hematopoietic Ba/F3 cell models rendered IL-3 independent by transduction with various constitutively active tyrosine kinases.<sup>18</sup> All compounds of the naphthalene-1-carboxamide series were 20- to 100-fold more potent than PTK787 and approximately the same order of magnitude as AAL993 and Sorafenib in the cellular Ba/F3 VEGFR2 assay (Table 4). In a series of additional Ba/F3 cell lines, all naphthalene-1-carboxamides targeted RET and PDGFRβ kinases in addition to VEGFR2, but displayed weak (> 1 μM) activity against other kinases such as FGFR3 and c-KIT (Table 4). Sorafenib and Sunitinib were less selective, generating IC<sub>50</sub> values for many of the kinases.

13

Ba/F3 line	BAW2881	BFH772	<u>4</u>	<u>9</u>	<u>10</u>	PTK787	AAL993	Sorafenib	Sunitinib
IC <sub>50</sub> (μM)									
Tel-KDR-	0.004 ±	0.002*	0.009 ±	0.002 ±	0.005 ±	0.215 ±	0.013 ±	0.014 ±	0.238 ±
myc1.3	0.001		0.002	0.001	0.002	0.043	0.004	0.0023	0.018
Bcr-ABL	4.748 ±	7.5**	>10	9.5**	>10	>10	>5.5	5.82 ±	7.177 ±
	0.844							0.237	2.534
NPM-ALK	>10	>10	>10	>10	>10	>10	>5.5	1.015 ±	1.154 ±
								0.12	0.1302
ERBB2	>10	>10	>10	>10	>10	>10	5.6*	4.208 ±	3.846 ±
(V659E)								0.173	0.572
Tel-FGFR3	8.271 ±	6.540 ±	8.257 ±	2.279 ±	2.658 ±	>10	>5.5	2.458 ±	1.561 ±
	0.988	0.290	0.091	0.041	0.054			0.156	0.295
FLT3-ITD	>10	>10	8.2*	5.646 ±	4.778 ±	>10	>5.5	0.012 ±	0.035 ±
				1.974	0.152			0.0021	0.0028
Tel-IGF-1R	>10	7.2**	8.9*	>10	>10	>10	8.4*	3.681 ±	1.289 ±
								0.881	0.412
KIT(D816V)	>10	>10	8.506 ±	8.0**	7.8**	>10	>5.5	2.804 ±	1.469 ±
			0.236					0.33	0.247
Trp-MET	>10	>10	>10	>10	>10	>10	>5.5	7.40 ±	5.124 ±
								0.786	0.101
PTC3-RET	0.152 ±	0.104 ±	0.226 ±	0.009 ±	0.040 ±	>10	2.9*	0.078 ±	0.297 ±
	0.036	0.026	0.005	0.002	0.012			0.012	0.0078
Tel-	0.009 ±	0.027 ±	0.016 ±	0.004 ±	0.010 ±	0.076 ±	0.019 ±	0.013 ±	0.0023 ±
PDGFRbeta	0.002	0.003	0.001	0.001	0.004	0.026	0.0055	0.0025	0.0007
WT (untrans-	>10	>10	>10	>10	>10	>10	>10	>10	>10
duced)									

14

**Table 4: Cellular selectivity in Ba/F3 assay** - The concentration-dependent effect of test compound on proliferation and viability of Ba/F3 cell models was determined by the resazurin sodium reduction assay. IC<sub>50</sub> values (μM) from at least two independent experiments, unless indicated otherwise, are presented as mean ± SEM. \*Only one determination. \*\*At least one replicate value > 10 μM. IC<sub>50</sub> is defined as the drug concentration inhibiting Ba/F3 cell viability to 50 % of that measured for vehicle-treated controls. All cells except parental Ba/F3-wt were grown in the absence of IL-3.

Taking these data together, overall this new series of compounds displayed selectivity against a panel of kinases comparable to PTK787 and AAL993, but more selective than Sorafenib and Sunitinib. The naphthalene-1-carboxamides were several fold more potent than PTK787 against VEGFR2. Interestingly, the naphthalene-1-carboxamides largely showed equal potency in the enzyme tyrosine kinase profiling and in cellular assays. This suggested that the compounds efficiently penetrated the cytoplasmic membrane of cells in the latter assay, a phenomenon that we have previously observed.<sup>19</sup>

#### **Activity in VEGF induced proliferation (Fig. 4)**

The naphthalene-1-carboxamides were subsequently tested in a functional assay before *in vivo* studies were initiated. In HUVEC endothelial cell proliferation assays, PTK787 was previously demonstrated to exhibit an IC<sub>50</sub> of 7.1 ± 5.1 nM against VEGF-induced proliferation.<sup>9, 15</sup> AAL993 and Sunitinib exhibited an IC<sub>50</sub> of 1 ± 0.16 nM and 7 ± 6 nM respectively, whereas the naphthalene-1-carboxamides were substantially more potent. IC<sub>50</sub> values of BAW2881 (0.12 ± 0.06 nM, n=4), compound **10** (0.003 ± 0.002 nM, n=2), BFH772 (<0.01 nM, n=2 see Fig. 4) and compound **4** (0.077 nM see Fig. 4) demonstrated that they abrogated VEGF induced proliferation at remarkably low nM concentrations. Compound **9** at IC<sub>50</sub> values of 1.7 ± 1.6 nM, n=2 was more similar to the anthranilic acid amide AAL993. The compounds were selective against VEGF induced proliferation. Only **10** revealed an IC<sub>50</sub> of 206 ± 44 nM (n=2) against FGF induced proliferation of HUVEC cells, which nevertheless was several orders of magnitude higher than for VEGF-induced proliferation. The other compounds were >3 μM against bFGF. We speculate that the reason for the extremely low IC<sub>50</sub> values

15

1  
2  
3  
4  
5  
6  
7  
8  
9  
10  
11  
12  
13  
14  
15  
16  
17  
18  
19  
20  
21  
22  
23  
24  
25  
26  
27  
28  
29  
30  
31  
32  
33  
34  
35  
36  
37  
38  
39  
40  
41  
42  
43  
44  
45  
46  
47  
48  
49  
50  
51  
52  
53  
54  
55  
56  
57  
58  
59  
60

obtained in the VEGF induced HUVEC proliferation assay are due to the fact that these compounds are able to penetrate the cytoplasmic membrane. Due to the relatively long duration (48 h) of the experiment, we hypothesized that the inhibitors accumulated in the endothelial cells and that this translated into the sub nanomolar efficacy. We were able to rule out potential cytotoxic effects since compounds started to affect viability of HUVEC cells as assessed by the YoPro assay only at 10  $\mu$ M and above (data not shown).

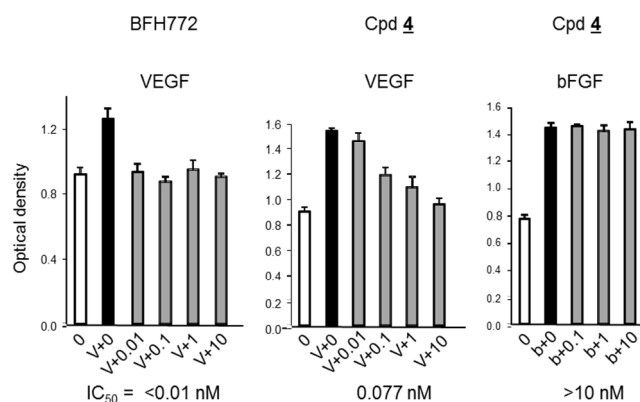


**Figure 4:** HUVEC proliferation assay in the presence of VEGF (10 ng/ml) (2 left hand graphs) or bFGF (0.5 ng/ml) (right hand graph). Basal proliferation shown with the white bar, and growth factor induced proliferation with the black bar. Compounds were added at the doses shown below the bars – eg V + 0.01 is VEGF plus 0.01 nM compound; b + 0.1 is bFGF plus 0.1 nM compound. BFH772 in the left hand graph shows full inhibitory activity at the lowest dose of 0.01 nM against VEGF induced proliferation. Cpd 4 is shown for comparison in the middle graph. Cpd 4 showed no activity against bFGF induced proliferation (right hand graph).

16

**Pharmacokinetics**

To determine whether the most potent cellular and biochemical VEGFR2 compounds of the 6-(pyrimidin-4-yloxy)-naphthalene-1-carboxylic acid phenylamides series were orally bioavailable, plasma concentrations were measured after administration to mice in a preliminary screen (not shown) and subsequently in rats as described.<sup>9, 15</sup> Even though manifesting low aqueous solubility only, most compounds showed exposure after oral administration (Fig. 5A). In the preliminary mouse PK screen, the potent cellular and biochemical VEGFR2 inhibitor compound **11**, showed a shorter half-life than compounds **4**, **10**, **9**, BFH772 and BAW2881. We hypothesized that **11** could be metabolically labile since it contains an ethyl side chain in its structure. As we had many other equipotent alternatives, we chose to deprioritize this inhibitor. Rat PK demonstrated that half-lives were variable with **10** having the longest duration of 18.3 h when applied intravenously. Graphs of 3 of the compounds, BAW2881, BFH772 and **4** are shown (Fig. 5B). The pharmacokinetic profile of the compounds suggested that this series would be suitable for testing in *in vivo* models.

17

**A**

Compound	Dose mg/kg	IV parameters			PO parameters (suspension)					
		CL L/h /kg	Vss L/kg	T <sub>1/2</sub> h	Dose mg/kg	t <sub>max</sub> h	C <sub>max, dn</sub> μmol/L	AUC <sub>0-Inf, dn</sub> μmol/L · h	T <sub>1/2</sub> h	BA %
<u>4</u>	3	0.17	3.5	16	50	5	0.07	1.37	10.1	9
<u>10</u>	3	0.05	1.5	18.3	50	8	0.08	4.19	nm	9
<u>9</u>	3	0.18	0.9	4.1	50	4	0.05	0.67	4.5	5
BFH722	1	0.18	0.63	2.5	3	2	1.57	13.2	4.1	46
BAW2881	2.5	0.66	1.3	2	25	2	0.28	1.22	2	35

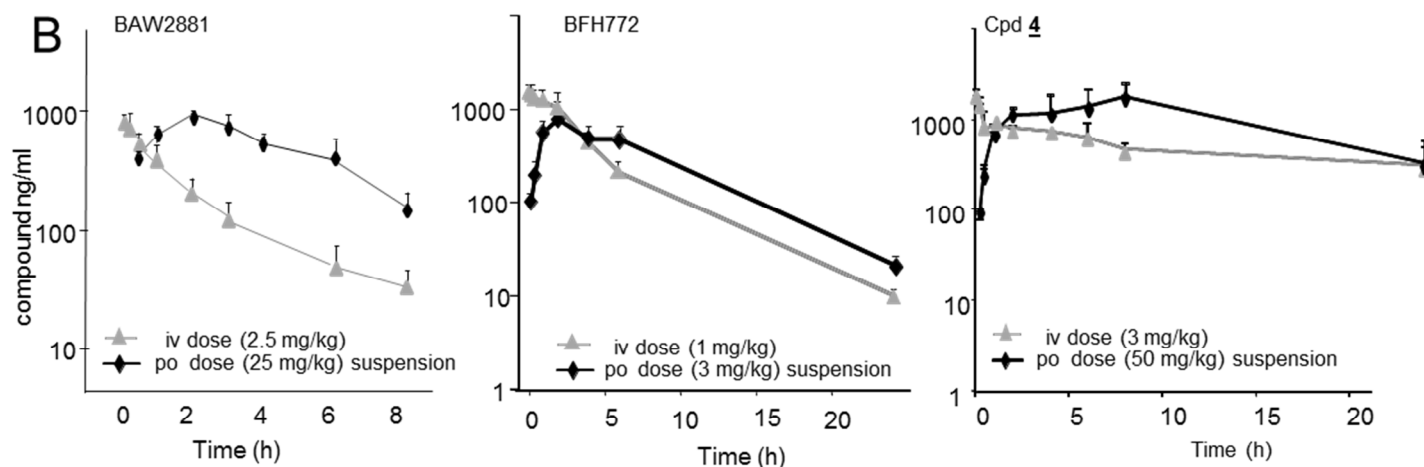


**Figure 5:** (A) – Table showing dose normalized (dn) PK parameters over 24 h in a set of rat PK experiments (female OFA rats for BAW2881 and BFH772; female Sprague Dawley rats for cpds **4**, **10**, and **9**). At 5, 15, 30 min, 1, 2, 4, 6, 8, and 24 h time points, drug concentrations in plasma was determined by HPLC/UV. Data represent SEM (n=2-4 animals per group). CL is clearance, Vss is volume of distribution at steady state. The value C<sub>max, dn</sub> represents the highest observed concentration (dose normalized) at the indicated time point (t<sub>max</sub>). T<sub>1/2</sub> is the half-life of the compounds exposure in plasma. AUC is the area under the curve – total exposure over 0 h → infinity, dose normalized. BA is percent bioavailability. nm is not measured. (B) – Example PK, time dependent exposure profiles for BAW2881 (n=4), BFH772 (n=2 for iv and n=3 for po) and cpd **4** (n=2 for iv and n=3 for po) shown. Grey triangles are iv administration, and black diamonds are p.o. dosing.

### Activity *in vivo*

18

**VEGF skin implant miles assay in mouse**

Two compounds of the naphthalene-1-carboxamide series were evaluated (**4** and BFH772) in a VEGF-induced vessel leakage miles assay<sup>20</sup> to confirm that the compounds would be suitable for dosing in longer term *in vivo* models. Doses were chosen based on rodent PK calculations and potency of the compounds in the various *in vitro* assays. For example, at 24 h, dose normalized exposure of compound **4** was 15 nM, for BAW2881 was 31 nM and for BFH772 was 83 nM, all of which were still more than the IC<sub>50</sub> value for VEGFR2 *in vitro*. We therefore opted to test inhibitors at 3 mg/kg initially since we expected that this would be sufficient to fully inhibit the VEGFR over the time period. Evans blue was injected intravenously into the mouse tail vein and 30 min later, 2 μL of dog VEGF164 (10 ng/μL) was injected intradermally into the dorsal pinna of the ear of the mouse. Vascular permeability was visualized by Evans blue extravasation measured with a computer assisted system. Compound **4** was applied 48, 24, and 8 h before sacrifice and BFH772 at 48 and 24 h before sacrifice. Compared to time 0, both VEGFR2 inhibitors, but especially **4** due to its long half-life substantially inhibited extravasation, even at 48 h prior to application of VEGF and Evans blue (Supplementary Fig. 3).

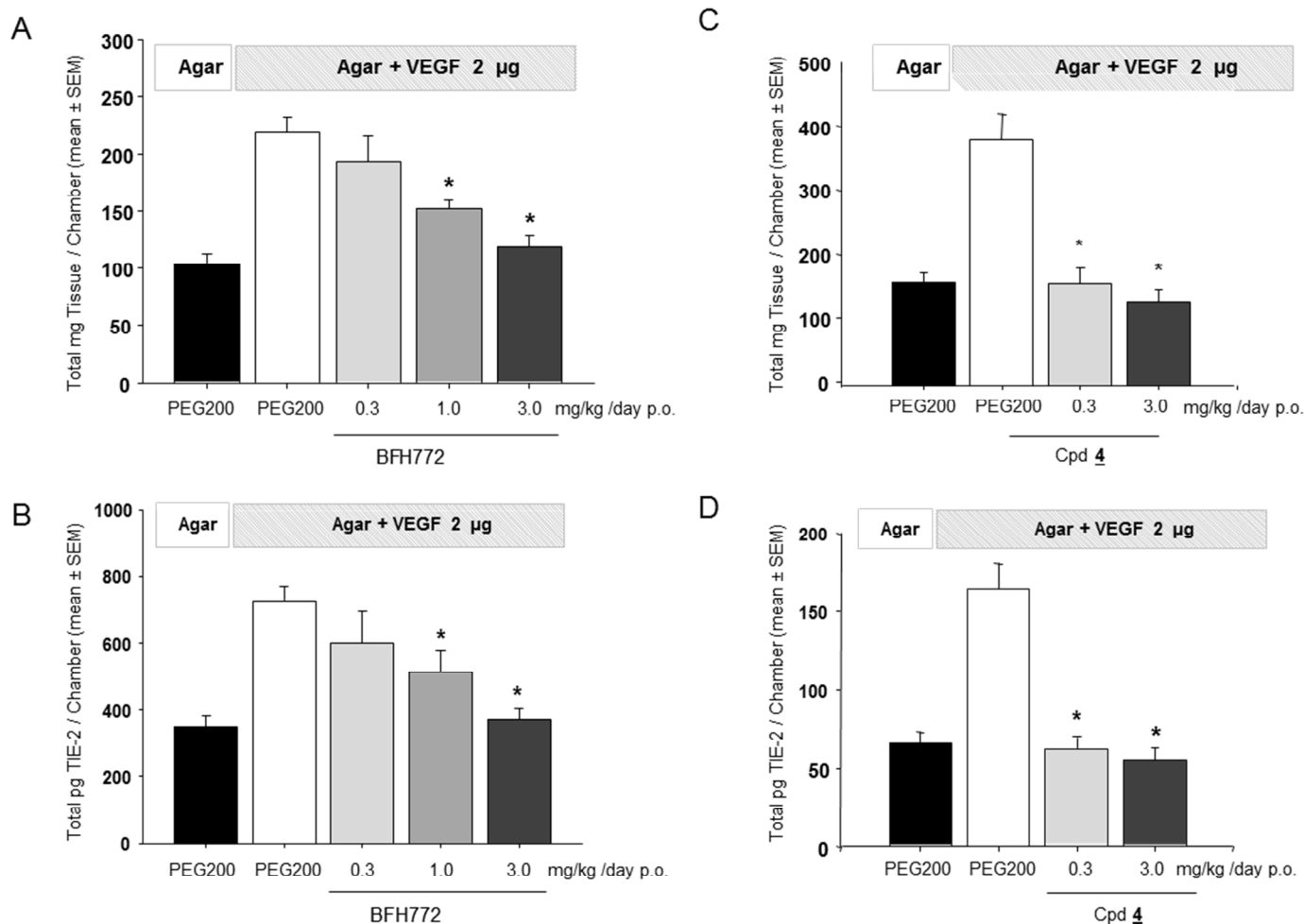
**VEGF-induced angiogenesis chamber model**

The miles assay gave us confidence to assess the compound activity in more complex long term *in vivo* models. The inhibition of a VEGF-mediated angiogenesis response after oral administration of the naphthalene-1-carboxamide inhibitors was measured in a growth factor chamber implant model in mice.<sup>9, 15</sup> Over a 4 day period, a new blood vessel-rich tissue is formed around the VEGF agar containing implanted chamber. This tissue can be removed, weighed and TIE-2 protein as a measure of endothelial cell amount and therefore vascularity, assessed in the lysate.

As BFH772 exhibited a good PK profile in rats with good C<sub>max</sub> and half-life characteristics as well as its potency and relative selectivity towards VEGFR2 *in vitro*, we considered this compound to be one of the best in the series. We also studied **4** in more detail as this compound exhibited a different profile to BFH772 in the pharmacokinetic analysis (mice), having an extended half-life of 10 h compared to 4 h for BFH772 but with a

19

1  
2 similar selectivity and potency in the *in vitro* profiling. Dose response curves of BFH772 at 0.3, 1 and 3 mg/kg  
3 demonstrated that even at the lowest concentrations, this naphthalene-1-carboxamide inhibited VEGF induced  
4 tissue weight and TIE-2 levels, but only reach statistical significance at 1 mg/kg and above (Figure 6 A and B).  
5  
6 Compound 4 on the other hand, already significantly reduced the tissue weight and TIE-2 levels back to basal at  
7 a dose of 0.3mg/kg (Figure 6 C and D). Other compounds of this series, 9, 10 and BAW2881 were also  
8  
9 substantially more potent than the two forerunners PTK787 (IC<sub>50</sub> of 30 mg/kg) and AAL993 (IC<sub>50</sub> 7 mg/kg)<sup>10</sup> on  
10  
11 tissue chamber weight (Supplementary Fig. 4 and data not shown). The mice tolerated the compounds well and  
12  
13 no signs of toxicity were observed. Vandetanib, (an EGFR, VEGFR and RET tyrosine kinase inhibitor  
14  
15 developed by Astra Zeneca) and SU6668 (a VEGFR, PDGFR, cKIT and bFGF inhibitor from Sugen) at 50  
16  
17 mg/kg inhibited tissue weight with similar efficacy to AAL993 and PTK787 (supplementary figure 4).  
18  
19  
20  
21  
22  
23  
24  
25  
26  
27



20

**Figure 6:** Dose response curve of BFH772 on tissue weight (A) and TIE-2 levels (B), and compound **4** on tissue weight (C) and TIE-2 levels (D). PEG200 vehicle treated animals were either implanted with agar chambers as a negative control (black bar) or with VEGF containing chambers as a positive control (white bar). BFH772 (0.3, 1 and 3 mg/kg) or compound **4** (0.3 and 3 mg/kg) treated mice were implanted with VEGF containing chambers (grey bars). Porous chambers containing VEGF (2  $\mu\text{g}/\text{mL}$ ) in 0.5 mL of 0.8 % w/v agar (containing heparin, 20 U/mL) were implanted subcutaneously in the flank of female FVB mice. Compounds were administered p.o. once daily in a vehicle of 100 % PEG200 (dose volume 5 mL/kg). Treatment was started 4-6 h before implantation of the chambers and continued for 4 days. The chambers were removed 24 h after the last dose. Each experiment was performed on groups of 6 mice per dose. Values are mean  $\pm$  SEM.

## Tumor models

### B16 melanoma

The anti-tumor activity of these naphthalene-1-carboxamides was evaluated in an orthotopic B16 melanoma model in B16/BL6 mice as described by LaMontagne *et al.*<sup>20</sup> A primary tumor forms in the ear where the cells are implanted and spontaneously formed cranial lymph node metastases occur in 100 % of the cases making this a very reproducible tumor model. Briefly, the highly metastatic subline B16/BL6 derived from B16 melanoma cells was injected intradermally under the skin of the ear of an anaesthetized mouse and primary tumor growth measured over the following 21 days. After this time, the mice were sacrificed and cranial lymph node metastases were excised and weighed.

21

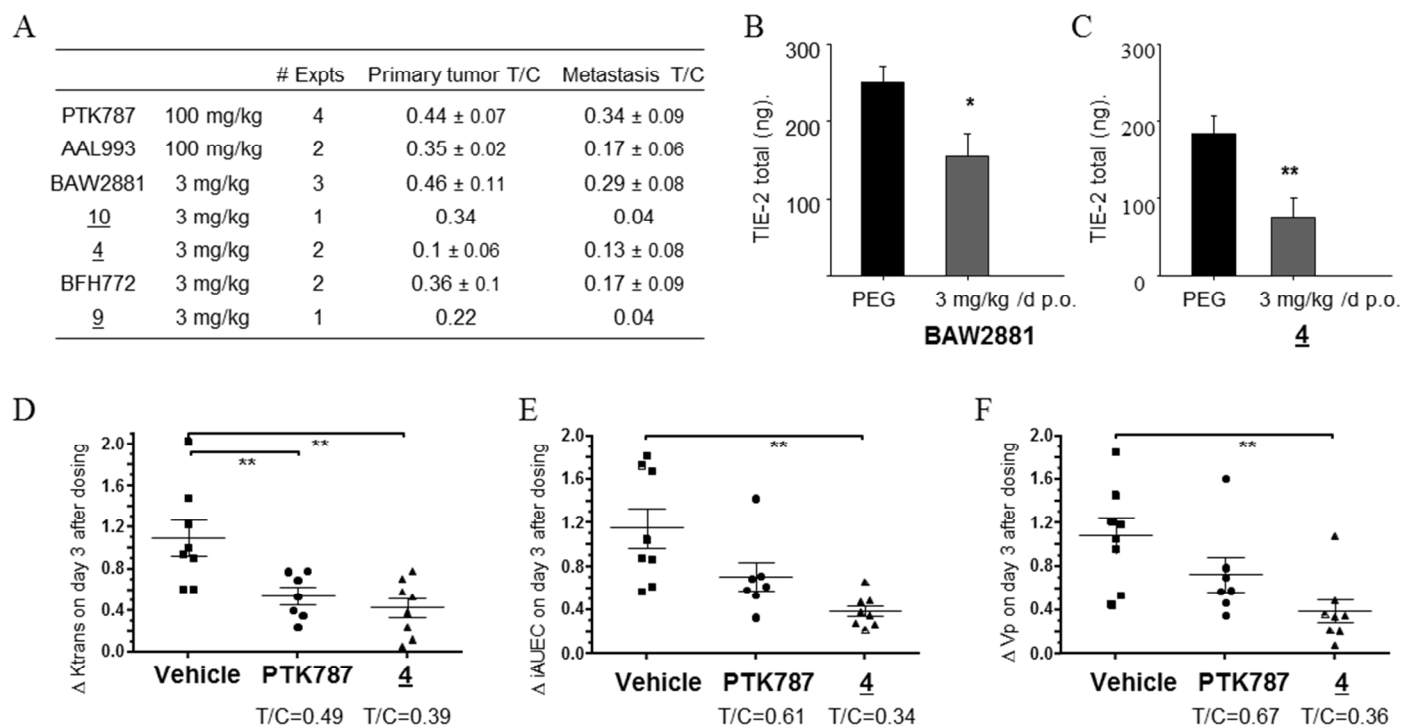


**Figure 7:** (A) – Table showing compound, dose, number of experiments performed and T/C (treatment/control) for B16 primary tumor growth and metastatic weights. Treatment was started at day 7 when the primary B16 tumor was already established after assignment of female C57Bl6 to groups of 5-6 animals with similar mean and range of tumor size. Primary tumor was measured with computer assisted imaging software. After two weeks of daily qd treatment (day 21 after cell injection) the animals were sacrificed and the cervical lymph nodes weighed. Vehicle was 100 % PEG 200. n=6 animals per group. (B) and (C) – TIE-2 levels in the lysates from metastases from the B16/BL6 melanoma model. Results from analysis of BAW2881 (B) and cpd **4** (C) shown. n= 6-12 animals per group. Values are mean ± SEM. \*p < 0.05, \*\*p<0.01 statistical significance of inhibition. (D-F) – DCE-MRI analysis of lymphnode metastases. The parameters determined by DCE-MRI of Ktrans (D), iAUEC (E) and Vp (F) show the changes in individual mice and the associated mean ± SEM (n=7-8 animals), with significance determined by a 1-way ANOVA, where \*p<0.05, \*\*p<0.01 compared to vehicle-treated mice.

BAW2881, **4**, **9**, **10** and BFH772 all at 3 mg/kg orally dosed once per day potently inhibited melanoma growth (by 54-90 % for primary tumor and 71-96 % for metastasis growth) as depicted by treatment to control ratios (Fig. 7A). At 3 mg/kg, the naphthalene-1-carboxamides showed the equivalent or better inhibition of primary and metastatic tumor growth that 100 mg/kg PTK787 could achieve. AAL993, Sunitinib and Sorafenib had to

22

1  
2  
3 be dosed at between 50-100mg/kg to attain similar efficacy while SU6668 and Vandetanib were substantially  
4  
5 less potent (Figure 7 and supplementary figure 5). The naphthalene-1-carboxamides were well tolerated, with  
6  
7 no obvious effects on the well-being or behavior of the mice. Body weight and spleen weight was unaffected by  
8  
9 the administration of the naphthalene-1-carboxamides compared to a healthy naive mouse (data not shown). At  
10  
11 the end of the experiment blood was taken from the animals to look for any cellular abnormalities. Blood  
12  
13 chemistry showed that mice with high tumor burden (vehicle treated animals) showed lower hematocrit levels  
14  
15 and red blood cell counts than compound treated animals probably due to the fact that the tumor was full of  
16  
17 leaky blood vessels providing an avenue for loss of blood components. Hematocrit levels and red blood cell  
18  
19 counts returned to normal non tumor bearing naïve mouse quantities in the naphthalene-1-carboxamide treated  
20  
21 animal blood, presumably due to the compounds efficacy and reduction in abnormal vasculature  
22  
23 (Supplementary Fig. 6 for BAW2881 and BFH772, others not shown). Other blood cell parameters measured  
24  
25 (white blood cells, platelets) were normal (Supplementary Fig.6 and data not shown).

26  
27  
28  
29  
30  
31  
32 Metastases were taken on day 21 and a protein lysate prepared from which TIE-2 levels as a measure of  
33  
34 endothelial cell content, was assessed by ELISA (Fig. 7B and C). In line with the reduced tumor volumes, the  
35  
36 naphthalene-1-carboxamides significantly reduced TIE-2 levels for BAW2881 and **4**. We ruled out any direct  
37  
38 effects of the naphthalene-1-carboxamides on proliferation rate of the B16 melanoma cells by incubating  
39  
40 compounds for 48 h with tumor cells and measuring BrdU incorporation (Supplementary figure 7). These data  
41  
42 suggest that the naphthalene-1-carboxamides rather than affecting tumor cells, targeted the tumor vasculature  
43  
44 thus starving the tumor of nutrients and stunting further growth.

45  
46  
47  
48  
49 Consistent with anti-angiogenic activity, **4**, and as previously described PTK787<sup>15</sup>, significantly reduced the  
50  
51 vascular permeability of B16 melanoma cervical metastases, as determined by DCE-MRI<sup>21</sup> (Fig7D-F). After 3-  
52  
53 days of daily treatment there was a highly significant decrease in Ktrans compared to baseline, of 51 % and 61 %  
54  
55 for PTK787 and **4** respectively. Furthermore, the tumour plasma volume (Vp) and the parameter normally  
56  
57  
58  
59  
60

23

utilized in the clinic to assess tumour blood-vessel permeability (iAUEC), were also significantly reduced by 4 by approximately 65 %, while PTK787 showed a non-significant trend for inhibition with decreases of 33-39 %.

We further performed dose response studies with BFH772 and **4** in the B16 melanoma model to estimate the minimal efficacious dose. In addition, since compound **4** had a half-life of just over 10 h, we were interested to investigate whether dosing on alternate days versus daily treatment impacted tumor growth (Figure 8).

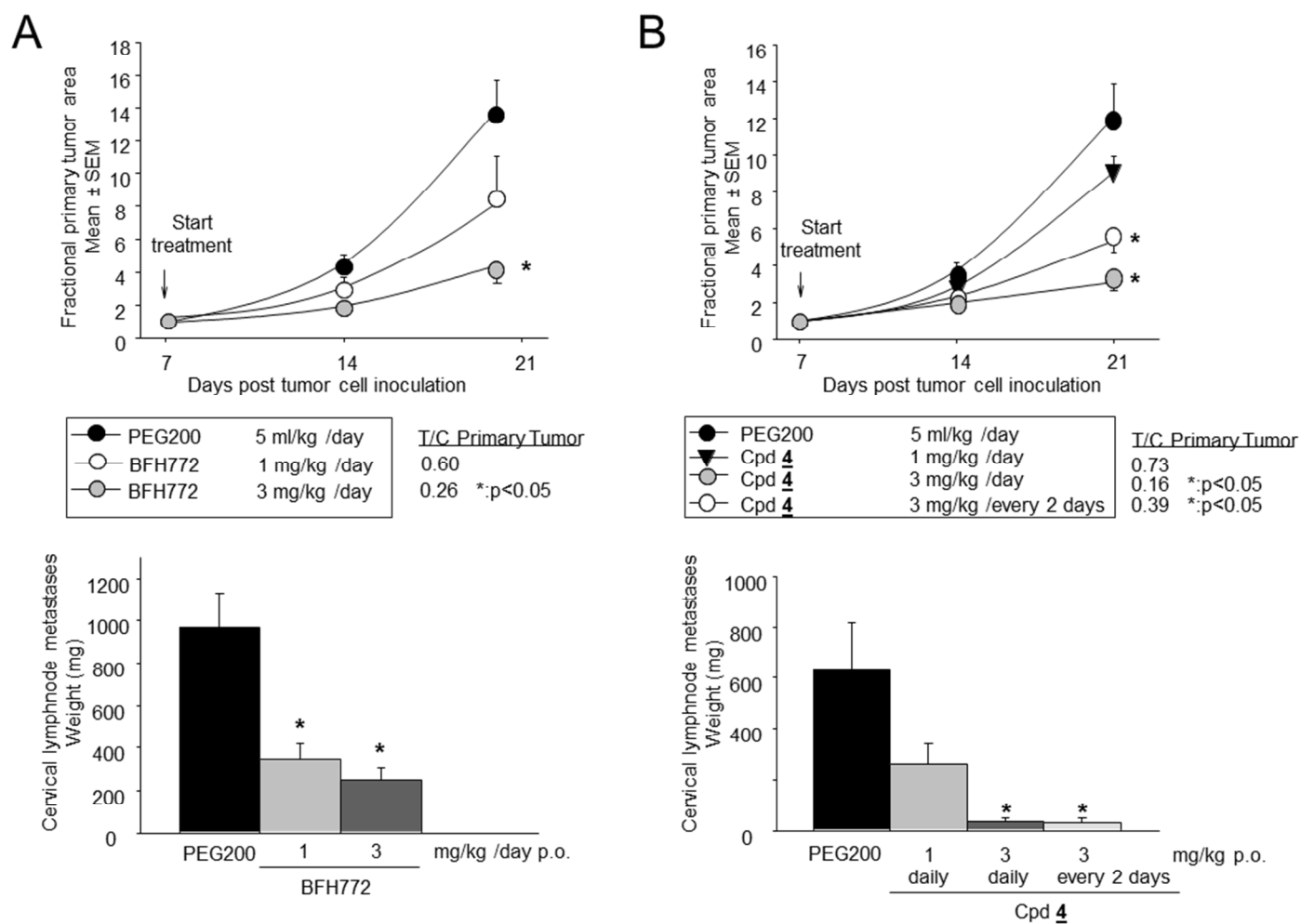


**Figure 8:** Effect of BFH772 (A) and compound **4** (B) on primary tumor growth rate and cervical lymphnode metastasis weight in the B16 melanoma model. Treatment was started at day 7 when the primary B16 tumor was already established after assignment of female C57B16 to groups of 6-10 animals with similar mean and range of tumor size. Primary tumor was measured with computer assisted imaging software. Vehicle was 100 % PEG 200. n=10 animals per group. BFH772 and compound **4** were 6 animals per group. BFH772 was dosed daily from treatment start. Compound **4** was dosed daily or once every 2 days from day 7. Significance determined by a 1-way ANOVA post Dunnett's test, where \*p<0.05, compared to vehicle-treated mice.

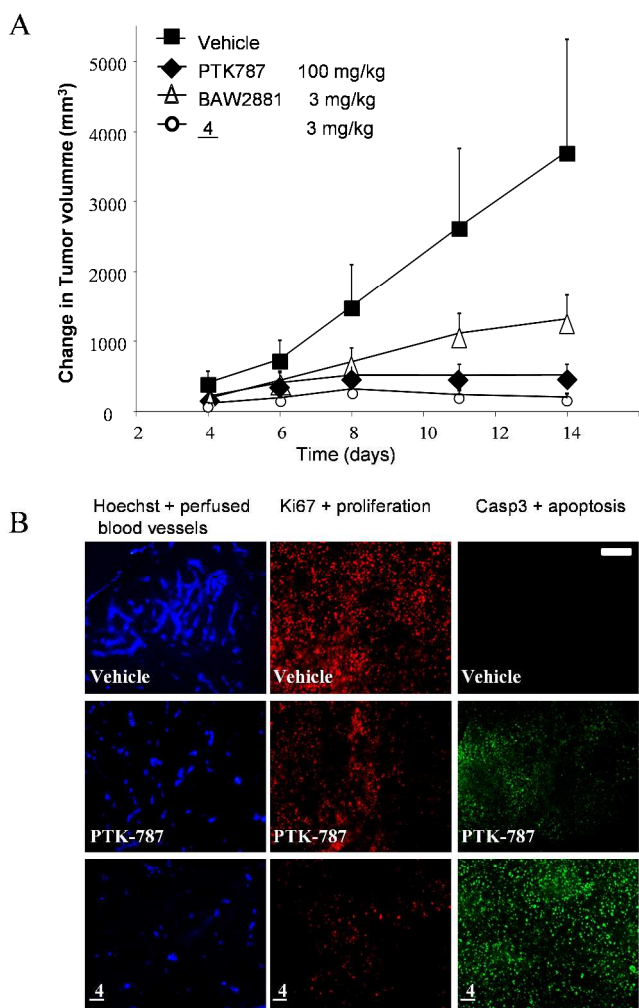
24

Both compounds inhibited primary and metastatic tumor growth at 3 mg/kg and BFH772 at 1 mg/kg reached statistical significance with regard to the metastasis weight. Interestingly, **4** when applied every 2 days at 3 mg/kg attained a statistically significant inhibition of both primary and metastatic tumor weight, the latter readout comparable to 3 mg/kg daily (Figure 8).

### **BN472 mammary carcinoma**

A second orthotopic tumor model using BN472 mammary carcinoma cells implanted into the breast pads of rats was performed with BAW2881 and **4**. Both compounds substantially inhibited tumor growth with BAW2881 showing a weaker efficacy than **4** with a T/C of 35.5 % versus 5.6 % respectively. In order to achieve the same level of inhibition, PTK787 had to be dosed at 100 mg/kg compared to 3 mg/kg for **4** (Fig. 9A) while AAL993 (100 mg/kg) was reported to inhibit tumor growth with a T/C value of 0.37<sup>16</sup> and Vandetanib (30 mg/kg), a T/C of 0.35. There were no significant effects on rat body-weight for any of the treatments (results not shown).

25



37 **Figure 9:** (A) – BN472 tumor growth curves over 14 days  
 38 with compounds treated qd,. Vehicle was PEG300. Female  
 39 Brown-Norway rats were randomized when tumor volume  
 40 was approximately 200 mm<sup>3</sup> before treatment started.  
 41 Experiment performed twice. n= 7-8 animals per group. (B) –  
 42 Histology of tumors after treatment with KDR inhibitors  
 43 PTK787 and cpd 4. Perfusable blood vessels were  
 44 highlighted by shortly injecting the animal with Hoechst dye  
 45 1 min before sacrifice (left panel of photomicrographs). 10  
 46 micron sections were stained with Ki67 to highlight tumor  
 47 proliferation (middle column) or caspase 3 to observe tumor  
 48 apoptosis (right column). Bar is 100 micron. All 3  
 49  
 50  
 51  
 52  
 53  
 54  
 55  
 56  
 57  
 58  
 59  
 60

26

1  
2 compounds caused a significant inhibition of tumour-growth  
3  
4 compared to vehicle by day-14 of treatment ( $p < 0.05$ , 2-way  
5  
6 RM-ANOVA).  
7

8  
9 Animals were injected intravenously with Hoechst dye shortly before sacrifice to highlight perfusable blood  
10  
11 vessels. Upon sacrifice, the tumors were excised and cryosections cut to visualize the Hoechst highlighted  
12  
13 vasculature, tumor proliferation with Ki67 staining and apoptosis with caspase 3 (Fig. 9B). Vehicle treated  
14  
15 tumors had a high blood vessel density which was substantially reduced in the PTK787 treated animals, and  
16  
17 further depleted in the **4**, and BAW2881 treatment groups (Fig. 9B left column, vehicle, PTK787 and **4** shown).  
18  
19 By targeting the vasculature in the tumor with the VEGFR2 kinase inhibitors, the environment is predicted to  
20  
21 become hypoxic leading to less proliferation and more apoptosis of the tumor cells. Indeed, less tumor  
22  
23 proliferation was observed in the PTK787 treated animals, a feature which was augmented with the  
24  
25 naphthalene-1-carboxamide series (middle column). Likewise, apoptosis of tumor cells was especially  
26  
27 promoted upon treatment with **4** (right column).  
28  
29  
30  
31  
32

33  
34 A further study with compound **4** applied at 3 mg/kg/day, 1 mg/kg/day and 1 mg/kg every two days to rats  
35  
36 bearing BN472 tumors revealed T/C ratios of 0.005, 0.028 and 0.176 respectively (data not shown). This  
37  
38 compound was therefore highly effective even when applied every other day.  
39  
40  
41  
42  
43  
44  
45  
46  
47

## 48 **Discussion and conclusion**

49  
50  
51 This paper describes the design and synthesis of a new and potent, highly selective series of VEGFR2 inhibitors.  
52  
53 Structure based morphing of the rather unselective FLT3 inhibitor AST487 led to the 6-(pyrimidin-4-yloxy)-  
54  
55 naphthalene-1-carboxamides, a class of potent VEGFR2 inhibitors being devoid of residual FLT3 activity. The  
56  
57 design was guided by the X-Ray structure of AAL993 complexed to VEGFR2. Herein the pyridine structure  
58  
59  
60

27

1  
2 element of AAL993 was replaced by an aminopyrimidine as we have observed for the hinge binding motif for  
3  
4 AST487. Subsequently, the anthranilic acid core of AAL993 was substituted by a naphthyl moiety. These  
5  
6 modifications maintained all the favorable interactions between inhibitor and the ATP binding pocket of  
7  
8 VEGFR2 and led to the BAW2881 series. In addition, to understand the selectivity profile of the 6-(amino-  
9  
10 pyrimidin-4-yloxy)-naphthalene-1-carboxamides, BAW2881 was docked into the respective homology model  
11  
12 of the kinase domain of FLT3 where it sterically clashed with the “gate keeper” residue. The binding hypothesis  
13  
14 based on the X-Ray structure of AAL993 bound to VEGFR2 explains the established SAR around the hinge  
15  
16 binding moiety of the 6-(pyrimidin-4-yloxy)-naphthalene-1-carboxamides: 2-Amino- (eg BAW2881), 6-amino-  
17  
18 (eg compound **9**) or 6-hydroxymethyl-pyrimidines (eg BFH772) are highly potent inhibitors for VEGFR2. In  
19  
20 contrast, bulkier hinge binders (compound **13**) or 2-amino-6-chloro-pyrimidines (compound **2**) are weaker  
21  
22 inhibitors.  
23  
24  
25  
26  
27  
28

29 In cellular assays, these compounds have low nanomolar potency against VEGFR2 and exhibit very little  
30  
31 activity towards other kinases with the exception of RET and PDGFR. Taking into account both cellular and  
32  
33 biochemical assays, other potential kinases targeted were RAF, a common mutation in many cancers, and  
34  
35 weaker TIE-2 and c-KIT. VEGFR2, TIE-2 and PDGFR are well established anti-angiogenesis targets by  
36  
37 disrupting the vasculature and surrounding pericytes.<sup>4,22</sup> RET mutations are often found in thyroid cancers<sup>23</sup>  
38  
39 while c-KIT mutations are associated with GIST<sup>24</sup> indicating that these tumor types would be potential  
40  
41 indications for the naphthalene-1-carboxamide series.  
42  
43  
44  
45

46 The high selectivity of our inhibitors gives them a potential advantage over the multi-kinase inhibitors in that  
47  
48 side effects should be reduced. Vandetanib, Sorafenib and Sunitinib target a broader spectrum of kinases and  
49  
50 although efficacious for cancers of the thyroid, kidney, GIST and liver, are associated with severe side effects  
51  
52 such as QT prolongation, cutaneous rash, and hand-and-foot skin reaction, necessitating drug interruption for  
53  
54 periods of time to allow the patient to recover. Although some of these side effects are not life threatening, they  
55  
56 do impair quality of life and raise the potential for tumors to regrow during the cessation of treatment.<sup>25</sup> On the  
57  
58  
59  
60

28

1  
2 other side, there is a growing body of evidence from the clinic that VEGFR2 therapy can rapidly lead to  
3  
4 resistance as the tumor microenvironment starts to depend upon other pathways.<sup>26</sup> How tumor cells  
5  
6 communicate with the stroma and vasculature is not fully understood. However, it is appreciated that interfering  
7  
8 with the cross talk between these with multi-kinase inhibitors, influences the tumor microenvironment and that  
9  
10 this may be a route to overcome drug resistance despite associated side effect profiles of these inhibitors.<sup>27</sup> The  
11  
12 fact that there are numerous multi-kinase inhibitors successfully treating cancer patients would suggest that  
13  
14 there is a benefit to targeting a broad spectrum of signaling pathways.  
15  
16  
17  
18

19  
20 The naphthalene-1-carboxamide compounds have the advantage that they are potent. They show reasonable  
21  
22 pharmacokinetic exposure and are able to inhibit VEGF-induced vascular leakage, VEGF-induced chamber  
23  
24 models and rodent orthotopic tumor models at doses as low as 3 mg/kg per day. BFH772 and compound **4** due  
25  
26 to their pharmacokinetic profile, stood out as the best two of the series, the latter compound due to its half-life  
27  
28 and exposure, able to show tumor weight inhibition when dosed every two days. As predicted by their mode of  
29  
30 action, the compounds target tissue vasculature as observed with TIE-2 ELISA levels in the tissue chamber  
31  
32 model, and vasculature by Hoechst perfusion in a tumor model. This ultimately leads to a lower tissue weight  
33  
34 growing around the implanted chamber, and an increase in tumor cell death accompanied by lower amounts of  
35  
36 proliferation in the tumor models respectively.  
37  
38  
39  
40

41  
42 Neoangiogenesis also plays an important role in other, non-cancerous diseases. Amongst them are inflammatory  
43  
44 skin disorders such as psoriasis. In this context, a strong inhibitory effect of BAW2881 in *in vitro* and *in vivo*  
45  
46 psoriasis preclinical models has been demonstrated; highlighting the fact that VEGF receptor kinase inhibitors  
47  
48 might be useful for the treatment of patients with inflammatory skin disorders.<sup>11c</sup> Furthermore, the inhibitory  
49  
50 effect of BFH772 in preclinical models of skin inflammation has also been described.<sup>11d</sup>  
51  
52  
53

54  
55 Our findings show that this new series of naphthalene-1-carboxamides display potent, p.o. active, and well-  
56  
57 tolerated inhibition of VEGF-mediated responses. With the caveats described above for selective kinase  
58  
59 inhibitors versus multi-kinase drugs, our compounds have the potential to be suitable, not only for cancers  
60

29

1  
2  
3 dependent on VEGF for their vascularization, but also for other diseases where VEGF-mediated angiogenesis  
4  
5 plays a crucial pathogenic role.  
6  
7  
8  
9  
10  
11  
12  
13  
14  
15  
16  
17  
18  
19  
20  
21  
22  
23  
24  
25  
26  
27  
28  
29  
30  
31  
32  
33  
34  
35  
36  
37  
38  
39  
40  
41  
42  
43  
44  
45  
46  
47  
48  
49  
50  
51  
52  
53  
54  
55  
56  
57  
58  
59  
60

30

## Experimental

### Materials

Human umbilical vein cells (HUVEC) were from PromoCell as were Endothelial cell growth medium Kit and Endothelial Cell Basal medium (BioConcept AG, Allschwil/Switzerland). They were used from passage 4 to 7. Compounds were all synthesized in the Department of Oncology Research (Novartis Pharmaceuticals). For *in vitro* assays, a stock solution of 10 mM compound was prepared in DMSO. This was diluted further in buffer or medium. The KDR-transfected CHO cells were obtained from the Institute of Molecular Medicine (Tumor Biology Center). For Ba/F3 cells, see reference.<sup>28</sup> VEGF<sub>164</sub> used for the chamber implant model, was from the Tumor Center, Freiburg Germany. TIE-2 ELISA was with a capture antibody, anti-TIE-2 AB33 (UBI, Hauppauge, NY). Detection antibody was with goat anti-mouse TIE-2 (R&D Systems, Minneapolis, MN) followed by alkaline phosphatase conjugated to monoclonal anti goat antibody (Sigma, St Louis, MO). TIE-2 complexes were detected by incubating with p-nitrophenyl phosphate (Sigma tablets). B16/BL6 melanoma cells were a kind gift from Dr. Isaiah J Fidler, Texas Medical center, Houston, TX. For immunohistochemistry, Hoechst dye was obtained from Sigma, rabbit anti mouse active caspase 3 was from Oncogene, Uniondale, NY and rabbit anti-mouse Ki67 was from Neomarkers, Fremont, CA. Secondary antibodies were goat anti-rabbit ALEXA 568 or 488 (Molecular Probes).

### Biology

#### *In vitro* kinase assay

*In vitro* kinase assays have been described by Wood *et al.*<sup>15</sup> Briefly the assay is based on a filter binding assay, using the recombinant GST-fused kinase domains expressed in baculovirus and purified over glutathione-Sepharose,  $\gamma$ -[<sup>33</sup>P]ATP as the phosphate donor, and poly-(Glu:Tyr 4:1) peptide as the acceptor. Each GST-fused kinase was incubated under optimized buffer conditions [20 mM Tris-HCl buffer (pH 7.5), 1–3 mM MnCl<sub>2</sub>, 3–10 mM MgCl<sub>2</sub>, 3–8  $\mu$ g/ml poly-(Glu:Tyr 4:1), 0.25 mg/ml polyethylene glycol 20000, 8  $\mu$ M ATP, 10  $\mu$ M

31

1  
2 sodium vanadate, 1 mM DTT], and 0.2 $\mu$ Ci  $\gamma$ -<sup>33</sup>P ATP in a total volume of 30  $\mu$ L in the presence or absence of a  
3  
4 test substance for 10 min at ambient temperature. The reaction was stopped by adding 10 mL of 250 mM EDTA.  
5  
6  
7 Using a 384-well filter system, half the volume was transferred onto an Immobilon-polyvinylidene difluoride  
8  
9 membrane (Millipore, Bedford, MA). The membrane was then washed extensively, dried and scintillation  
10  
11 counting was performed. IC<sub>50</sub>s for compounds were calculated by linear regression analysis of the percentage  
12  
13 inhibition.  
14  
15

#### 16 17 Cellular VEGFR2 autophosphorylation assays

18  
19  
20 CHO and HUVEC VEGFR2 assays were performed as described by Wood *et al.*<sup>15</sup> Briefly cell-based receptor  
21  
22 autophosphorylation assays using HUVECs that naturally express VEGFR2 or VEGFR2-transfected CHO cells  
23  
24 were used. The cells were seeded in six-well plates and grown to 80 % confluency. Compound was added in  
25  
26 serial dilutions, and the cells incubated for 2 h at 37 °C in medium without FCS. VEGF (20 ng/mL) was then  
27  
28 added. After 5 min incubation (37 °C), cells were washed and lysed. Nuclei were removed by full-speed  
29  
30 centrifugation for 10 min at 4 °C using an Eppendorf-centrifuge. Protein concentrations of the lysates were  
31  
32 determined. A monoclonal antibody to VEGFR2 (monoclonal antibody 1495.12.14; Novartis) was coated to  
33  
34 microtiter plates as a capture antibody. Cell lysates were added in triplicate together with an alkaline  
35  
36 phosphatase-labeled anti-phosphotyrosine antibody (PY-20(AP), Transduction Laboratories, Lexington, KY).  
37  
38 After overnight incubation at 4 °C, the bound PY-20(AP) was detected with a luminescent alkaline phosphatase  
39  
40 substrate (TROPIX, Bedford MA), and chemiluminescence was then determined.  
41  
42  
43  
44  
45  
46  
47

#### 48 Ba/F3 proliferation assays

49  
50 Different Ba/F3 cell lines rendered IL-3 independent by transduction with various constitutively active tyrosine  
51  
52 kinases were grown in RPMI 1640 medium containing 10 % fetal calf serum. For maintenance of parental  
53  
54 Ba/F3 cells the medium was additionally supplemented with 10 ng/mL interleukin-3 (IL-3; Biosource). For  
55  
56 proliferation assays, Ba/F3 cells were seeded on 96-well-plates in triplicates at 10000 cells per well and  
57  
58 incubated with various concentrations of compounds for 72 h followed by quantification of viable cells using a  
59  
60

32

1  
2 resazurin sodium salt dye reduction readout (commercially known as AlamarBlue assay). IC<sub>50</sub> values were  
3  
4 determined with the XLFit Excel Add-In (ID Business Solutions) using a 4-parameter dose response model.  
5  
6

7  
8 Endothelial cell proliferation assays.  
9

10  
11 As a test of the ability of compounds to inhibit a functional response to VEGF, an endothelial cell proliferation  
12  
13 assay, based on BrdUrd incorporation was used (Biotrak Cell Proliferation System V.2, Amersham, England) as  
14  
15 described previously.<sup>15</sup> Briefly subconfluent HUVECs were incubated in triplicate in 96-well plates with basal  
16  
17 medium containing 1.5 % FCS and a constant concentration of VEGF (10 ng/ml), bFGF (0.5 ng/mL), or FCS  
18  
19 (5 %), in the presence or absence of compounds. After 24 h of incubation, BrdUrd labeling solution was added,  
20  
21 and cells incubated an additional 24 h before fixation, blocking, and addition of peroxidase-labeled anti-BrdUrd  
22  
23 antibody. Bound antibody was then detected spectrophotometrically at 450 nm.  
24  
25  
26  
27  
28  
29  
30  
31

### 32 *In vivo* studies

33

34 All mice and rats were used with strict adherence and in accordance with Swiss Federal and Cantonal  
35  
36 Authorities. Animals were kept under standard conditions (optimal health conditions, 22 °C in special,  
37  
38 acclimatized animal rooms with 12 h dark-light cycles, light from 0600 to 1800) with free access to tap water  
39  
40 and pelleted rodent chow.  
41  
42  
43  
44  
45

### 46 Rat pharmacokinetics

47

48  
49 Catheters were implanted into the femoral artery and vein of naïve female rats strain OFA for BFH772, and  
50  
51 BAW2881, or in the jugular vein and femoral artery in female Sprague Dawley rats for compounds **4**, **9** and **10**.  
52  
53  
54 Animals were allowed to recover for 96 h, and were housed in single cages with free access to food and water  
55  
56 throughout the experiment. Female OFA rats received 2.5 mg/kg of BAW2881 dissolved in  
57  
58 ethanol/dimethylisorbide/polyethyleneglycol400/D5W (10/15/35/40 v/v) or 1mg/kg of BFH772 dissolved in  
59  
60

33

1  
2 N-methyl pyrrolidone/polyethyleneglycol200 (30:70, v/v) via injection into the femoral vein. D5W is glucose 5 %  
3 / water (v/v). Oral administration: BAW2881 and BFH772 were formulated as a micronized suspension  
4  
5 (dissolved/suspended in 0.5 % carboxymethyl cellulose in distilled water) and administered by gavage to female  
6  
7 OFA rats to deliver a dose of 25 mg/kg for BAW2881 or 3 mg/kg BFH772. (n=4 rats per group). For  
8  
9 compounds **4**, **9** and **10**, female Sprague Dawley rats at 8 weeks of age, received an intravenous dose of 3  
10  
11 mg/kg **4**, **9** and **10**, formulated in ethanol/NMP/polyethyleneglycol400/D5W (10/10/50/30) (n=2 rats per group),  
12  
13 or a suspension in 0.5 % carboxymethyl cellulose in distilled water dosed at 50 mg/kg (n=3 rats per group). At  
14  
15 the allotted times, blood samples were collected into heparinized tubes and the amount of compound in plasma  
16  
17 determined by HPLC/MS-MS.  
18  
19  
20  
21  
22  
23  
24  
25  
26

#### 27 Tissue chamber model and TIE-2 ELISA

28  
29 Female FVB mice weighing between 18 to 20 g were housed in groups of 6. Porous chambers containing VEGF  
30  
31 (2 µg/mL) in 0.5 mL of 0.8 % w/v agar (containing heparin, 20 U/mL) were implanted subcutaneously in the  
32  
33 flank of the mice, (n=6 per group). VEGF induces the growth of vascularized tissue around the chamber. This  
34  
35 response is dose-dependent and can be quantified by measuring the weight and TIE-2 levels of the tissue. Mice  
36  
37 were treated either orally once daily with compounds or vehicle (PEG200 100 %, 5 mL/kg) starting 4-6 h before  
38  
39 implantation of the chambers and continuing for 4 days. The animals were sacrificed for measurement of the  
40  
41 vascularized tissues 24 h after the last dose. Tissue weight was taken and then a lysate prepared for TIE-2  
42  
43 ELISA analysis as described by LaMontagne *et al.*<sup>20</sup>  
44  
45  
46  
47  
48  
49  
50  
51

#### 52 Miles assay<sup>20</sup>

34

1  
2  
3 Female FVB mice weighing between 18 to 20 g were housed in groups of 3-4. Compound was administered to  
4  
5 the mice at various time points before injection of Evans blue (48, 24, 8, and 2 h before). 200  $\mu$ l of Evans blue  
6  
7 0.5 % was injected i.v. in the tail vein of FVB mice. 30 min later, 2  $\mu$ L of dog VEGF164 (10 ng/ $\mu$ L) was  
8  
9 injected intradermally into the dorsal pinna of one ear of the mouse. 30 min later, pictures of the ear were taken.  
10  
11 Albumin-bounded Evans blue dye will extravasate at sites of increased microvascular permeability, generating a  
12  
13 visible blue spot which provides a measure of vascular permeability. Measurements of the dye extravasation  
14  
15 area ( $\text{mm}^2$ ) were carried out using pixel-based threshold in a computer-assisted image analysis software (KS-  
16  
17 400 3.0 imaging system, Zeiss, Germany). (n=3-4 animals per group).  
18  
19  
20  
21  
22  
23

#### 24 B16/BL6 murine melanoma tumor model

25  
26 This model has been described by LaMontagne *et al.*<sup>20</sup> The B16/BL6 melanoma cells are a subline from B16  
27  
28 cells with a highly aggressive metastatic capability and were a kind gift from Dr Isaiah J. Fidler, Texas Medical  
29  
30 centre, Houston, TX, USA. Briefly 50000 tumor cells were injected intradermally in the dorsal pinna of both  
31  
32 ears of female C57BL/6JNpa mice, (weighing between 18 to 20 g). Primary tumor size was measured on day 7,  
33  
34 14 and 21 in  $\text{mm}^2$  with a computer assisted image analysis software (KS-400 3.0 imaging system, Zeiss) and a  
35  
36 specifically designed macro. Animals were randomized into cages with groups of 5-6 so that they had roughly  
37  
38 equal primary tumor size on day 7 and treated with the compounds or vehicle PEG300 or PEG200 daily p.o. for  
39  
40 the following 14 days. On day 21, mice were sacrificed and cranial lymph nodes excised and weighed. Blood  
41  
42 was taken and measured directly by a blood analyser which determines platelet, red and white blood cell counts  
43  
44 as well as hematocrit levels.  
45  
46  
47  
48  
49  
50  
51  
52  
53  
54

#### 55 DCE-MRI

56  
57  
58  
59  
60

35

1  
2 Dynamic-contrast-enhanced MRI (DCE-MRI) was performed exactly as previously described.<sup>21</sup> Cohorts of at  
3  
4 least 8 C57BL/6JNpa B16 tumor bearing mice per group were anaesthetized, contrast-agent injected and the  
5  
6 parameters of Ktrans, and iAUEC (both for tumour vessel permeability) and Vp (tumour plasma volume) of the  
7  
8 cervical lymph-node metastases determined. Mice were then treated daily with vehicle, PTK787 or **4** and the  
9  
10 procedure repeated. The change in the individual parameter for each mouse was recorded and results shown the  
11  
12 individual values for each parameter and the associated mean±SEM, with a one-way-ANOVA used to  
13  
14 determine significance (Holm-Sidak multiple-comparisons).  
15  
16  
17  
18  
19  
20  
21

22 BN472 model

23  
24 Female Brown-Norway rats weighing 160 to 180 g were transplanted with 3 mm<sup>3</sup> tumor fragments of BN472  
25  
26 tumors in the mammary fat pads as described by Ferretti *et al.*<sup>29</sup> Tumors were used for efficacy studies at 2 to 3  
27  
28 weeks after transplantation when the tumor had reached 200 mm<sup>2</sup>. Rats were randomized into different groups  
29  
30 of 7-8 animals and treated orally with vehicle (PEG300) or compound.  
31  
32  
33  
34  
35

36 Immunohistochemistry and visualization of blood vessels

37  
38 Hoechst dye was injected into the Brown-Norway rats i.v. 2 min before sacrifice and excision of tumors.  
39  
40 Metastases were embedded in OCT cryosection embedding compound and 10 micron frozen sections cut.  
41  
42 Hoechst stained perfusable vasculature could be directly viewed if slides were mounted directly. Alternatively  
43  
44 sections of metastases were then blocked for 30 min with 10 % normal goat serum (NGS) in PBS containing  
45  
46 0.1 % Triton X-100, and incubated overnight at 4 °C or for 2 h at room temperature with various dilutions of the  
47  
48 primary antibodies in 3 % NGS and 0.1 % Triton-X100 in PBS. Primary antibodies were rabbit anti rat Ki67  
49  
50 (Neo Markers 1:200 dilution) and rabbit anti rat caspase 3 (Oncogene 1:10 dilution). To the washed sections (3  
51  
52 x 5 min) were added TRITC or FITC conjugated secondary antibodies in PBS containing 3 % NGS and 0.1 %  
53  
54 Triton X-100. Sections were incubated for 1 h at room temperature before washing 3 x 5 min in PBS and  
55  
56  
57  
58  
59  
60

36

mounting in mowiol. Images were collected with the Hamamatsu digital camera using a Zeiss (axioplan) microscope connected to the open-lab imaging system program.

## Chemistry

All reactions were performed under an inert atmosphere of N<sub>2</sub>. Starting materials were used as received from commercial sources. The purity ( $\geq 95\%$ ) of final compounds was verified by HPLC and <sup>1</sup>H-NMR analysis. None of the compounds showed any clear cut hydroscopic behavior. Column flash chromatography was performed on silica gel 60 (230-400 mesh ASTM, E. Merck). Melting points were determined in an open capillary and are not corrected. <sup>1</sup>H-NMR spectra were collected with Bruker DRX-500 (500 MHz), Bruker AM-360 (360 MHz) or Varian Gemini-300 (300 MHz) instruments; chemical shifts of signals are expressed in parts per million (ppm) and are referenced to the deuterated solvents used. MS spectra were collected with an FAB-ZAB, HF (VG Analytical). HPLC spectra were recorded on a Waters Ultra Performance LC instrument.

Abbreviations: aq. (aqueous); brine (saturated NaCl solution); DABCO (1,4-diazabicyclo[2.2.2]octane); DEPC (diethyl cyanophosphonate); DMAP (4-dimethylamino-pyridine); org. (organic); rt (room temperature); rv (rotary evaporation); T3P<sup>®</sup> (N-propylphosphonic acid anhydride, cyclic trimer [Cas: 68957-94-8]; 50 % in DMF)

**6-(2-Amino-6-chloro-pyrimidin-4-yloxy)-naphthalene-1-carboxylic acid (1):** To a mixture of 1 N aq. NaOH (160 mL) and acetone (320 mL) were added 2-amino-4,6-dichloro-pyrimidine (13.1 g; 80 mmol) and 6-hydroxy-1-naphthoic acid (15 g; 80 mmol). The mixture was stirred for 40 h at 62 °C. The cooled reaction mixture was partially evaporated by rv and the residue poured into 3 kg ice-water. Acidification with 2 N aq. HCl (42 mL; pH 4) and stirring gave solide **1**, which was isolated by filtration and washing with water (23 g; 91 %): MS: [M+1]<sup>+</sup> = 316; <sup>1</sup>H-NMR (DMSO-d<sub>6</sub>);  $\delta$  [ppm]: 8.93 (1H, d, *J*=9 Hz), 8.16 (2H, m), 7.87 (1H, d, *J*=2 Hz), 7.64 (1H, t, *J*=8 Hz), 7.53 (1H, dd, *J*=9 Hz / 2 Hz), 7.17 (2H, sb), 6.38 (1H, s).

**6-(2-Amino-6-chloro-pyrimidin-4-yloxy)-naphthalene-1-carboxylic acid (3-trifluoromethyl-phenyl)-amide (2):** Compound **1** (3.50 g; 11.1 mmol) was dissolved in DMF (60 mL) and cooled in an ice-bath. 4-

37

Methylmorpholine (1.72 mL; 15.8 mmol) and DEPC (3.04 mL; 20 mmol) were added. After 2 min 3-trifluoromethyl-aniline (1.52 mL; 12.2 mmol) was added and the mixture stirred for 21 h at rt. The reaction mixture was concentrated *in vacuo* and the residue re-dissolved in EtOAc and water. The aq. layer was separated off and re-extracted with EtOAc (2x). Washing the org. layers with water and brine, drying (Na<sub>2</sub>SO<sub>4</sub>), evaporation and column chromatography (SiO<sub>2</sub>; hexane/EtOAc 9:1 → 1:1) gave **2** (3.13 g; 61 %): MS: [M+1]<sup>+</sup> = 459; <sup>1</sup>H-NMR (DMSO-d<sub>6</sub>); δ [ppm]: 10.96 (1H, s), 8.34 (1H, s), 8.29 (1H, d, *J*=9 Hz), 8.13 (1H, d, *J*=8 Hz), 8.04 (1H, d, *J*=8 Hz), 7.88 (1H, s), 7.84 (1H, d, *J*=7 Hz), 7.69 (2H, m), 7.51 (2H, m), 7.17 (2H, sb), 6.38 (1H, s).

#### **6-(2-Amino-pyrimidin-4-yloxy)-naphthalene-1-carboxylic acid (3-trifluoromethyl-phenyl)-amide**

**(BAW2881)**: A mixture of **2** (3.13 g; 6.82 mmol), Pd/C 10 % (1.9 g), NEt<sub>3</sub> (1.04 mL; 7.5 mmol) and THF (330 mL) was hydrogenated at normal pressure. The catalyst was filtered off and the filtrate concentrated. The residue was re-dissolved in EtOAc and water. The aq. layer was separated off and re-extracted with EtOAc (2x). Washing the org. layers with water and brine, drying (Na<sub>2</sub>SO<sub>4</sub>), concentration and column chromatography (SiO<sub>2</sub>; toluene/acetone 4:1 → 3:2) gave BAW2881 (2.17 g; 75 %): mp: 218 °C; MS: [M+1]<sup>+</sup> = 425; <sup>1</sup>H-NMR (DMSO-d<sub>6</sub>); δ [ppm]: 10.96 (1H, s), 8.35 (1H, s), 8.28 (1H, d, *J*=9 Hz), 8.19 (1H, sb), 8.12 (1H, d, *J*=8 Hz), 8.04 (1H, d, *J*=8 Hz), 7.84 (2H, m), 7.67 (2H, m), 7.48 (2H, m), 6.66 (2H, sb), 6.25 (1H, d, *J*=5 Hz).

**6-(2-Amino-pyrimidin-4-yloxy)-naphthalene-1-carboxylic acid (3)**: A mixture of **1** (24.3 g; 77 mmol), Pd/C 10 % (15 g), NEt<sub>3</sub> (100 mL) and THF (3.5 L) was hydrogenated at normal pressure. The catalyst was filtered off and washed thoroughly with THF. Partial evaporation of the filtrate led to crystallization. Filtration and washing with THF gave **3** (10.0 g; 46 %): MS: [M+1]<sup>+</sup> = 282; <sup>1</sup>H-NMR (DMSO-d<sub>6</sub>); δ [ppm]: 8.93 (1H, d, *J*=9 Hz), 8.15 (3H, m), 7.83 (1H, s), 7.63 (1H, t, *J*=8 Hz), 7.50 (1H, d, *J*=9 Hz), 6.65 (2H, s), 6.24 (1H, d, *J*=5 Hz).

#### **6-(2-Amino-pyrimidin-4-yloxy)-naphthalene-1-carboxylic acid (4-fluoro-3-trifluoromethyl-phenyl)-amide**

**(4)**: Compound **3** (2.1 g; 7.8 mmol) was suspended in DMF (50 mL). Et<sub>3</sub>N (11 mL; 79 mmol), DMAP (0.42 g; 3.4 mmol), 4-fluoro-3-trifluoromethyl-aniline (1.6 mL; 9.7 mmol) and T3P<sup>®</sup> (9.1 mL; 15.6 mmol) were added. The reaction mixture was stirred for 1 h at rt, concentrated *in vacuo* and the residue re-dissolved in EtOAc and

38

1  
2 water. The aq. layer was separated off and re-extracted with EtOAc (2x). Washing the org. layers with water  
3  
4 and brine, drying (Na<sub>2</sub>SO<sub>4</sub>), evaporation and column chromatography (SiO<sub>2</sub>; CH<sub>2</sub>Cl<sub>2</sub>/EtOAc 4:1 → 1:2) gave **4**  
5  
6 (2.0 g; 59 %): mp: 204-205 °C; MS: [M+1]<sup>+</sup> = 443; <sup>1</sup>H-NMR (DMSO-d<sub>6</sub>); δ [ppm]: 10.97 (1H, s), 8.36 (1H, m),  
7  
8 8.29 (1H, d, *J*=9 Hz), 8.17 (1H, d, *J*=5 Hz), 8.11 (2H, m), 7.86 (1H, d, *J*=2 Hz), 7.83 (1H, d, *J*=6 Hz), 7.68 (1H,  
9  
10 t, *J*=8 Hz), 7.59 (1H, m), 7.47 (1H, dd, *J*=9 Hz / 2 Hz), 6.66 (2H, sb), 6.25 (1H, d, *J*=5 Hz).  
11  
12

13  
14  
15 **6-(2-Amino-pyrimidin-4-yloxy)-naphthalene-1-carboxylic acid [4-(4-methyl-piperazin-1-ylmethyl)-3-**  
16  
17 **trifluoromethyl-phenyl]-amide (5)**: Compound **5** was prepared analogously to **4** (112 mg; 36 %): MS: [M+1]<sup>+</sup>  
18  
19 = 437; <sup>1</sup>H-NMR (CD<sub>3</sub>OD-d<sub>4</sub>); δ [ppm]: 8.37 (1H, d, *J*=9 Hz), 8.23 (1H, s), 8.14 (1H, d, *J*=6 Hz), 8.07 (1H, d,  
20  
21 *J*=8 Hz), 8.00 (1H, d, *J*=9 Hz), 7.82 (2H, m), 7.77 (1H, s), 7.65 (1H, t, *J*=8 Hz), 7.45 (1H, d, *J*=9 Hz), 6.30 (1H,  
22  
23 d, *J*=6 Hz), 3.72 (2H, s), 2.59 (8H, m), 2.36 (3H, s).  
24  
25  
26  
27

28 **{4-[5-(4-Fluoro-3-trifluoromethyl-phenylcarbonyl)-naphthalen-2-yloxy]-pyrimidin-2-yl}-carbamic acid**  
29  
30 **methyl ester (6)**: Compound **4** (300 mg; 0.68 mmol) was dissolved in CH<sub>2</sub>Cl<sub>2</sub> (4.5 mL) and pyridine (7.5 mL).  
31  
32 Then methyl chloroformate (126 μL; 1.63 mmol) dissolved in CH<sub>2</sub>Cl<sub>2</sub> (2 mL) was added portion-wise. After 4 h  
33  
34 the reaction mixture was diluted with EtOAc and water. The aq. layer was separated off and re-extracted with  
35  
36 EtOAc (2x). Washing the org. layers with water and brine, drying (Na<sub>2</sub>SO<sub>4</sub>) and evaporation led to  
37  
38 crystallization of the product. After addition of *i*-Pr<sub>2</sub>O **6** was filtered off (243 mg; 71 %): mp: 199-200 °C; MS:  
39  
40 [M+1]<sup>+</sup> = 501; <sup>1</sup>H-NMR (DMSO-d<sub>6</sub>); δ [ppm]: 10.98 (1H, s), 10.42 (1H, s), 8.53 (1H, d, *J*=5 Hz), 8.37 (1H, m),  
41  
42 8.31 (1H, d, *J*=9 Hz), 8.13 (1H, d, *J*=9 Hz), 8.10 (1H, m), 8.05 (1H, d, *J*=2 Hz), 7.85 (1H, d, *J*=7 Hz), 7.70 (1H,  
43  
44 t, *J*=8 Hz), 7.58 (2H, m), 6.78 (1H, d, *J*=5 Hz), 3.60 (3H, s).  
45  
46  
47  
48  
49

50  
51 **6-(6-Chloro-pyrimidin-4-yloxy)-naphthalene-1-carboxylic acid (7)**: To a mixture of 1 N aq. NaOH (80 mL)  
52  
53 and acetone (100 mL) were added 6-hydroxy-1-naphthoic acid (7.5 g; 40 mmol). Then a solution of 4,6-  
54  
55 dichloro-pyrimidine (5.96 g; 40 mmol) in acetone (60 mL) was added dropwise. The mixture was stirred for 3 h  
56  
57 at rt and then partially concentrated by *rv*. The residue was poured into 1.6 kg ice-water. Acidification with 2 N  
58  
59 aq. HCl (20 mL; pH 4) and stirring at 0 °C gave solide **7**, which was filtered off and washed with water (10.5 g;  
60

39

87 %): MS:  $[M+1]^+ = 301$ ;  $^1\text{H-NMR}$  (DMSO- $d_6$ );  $\delta$  [ppm]: 8.99 (1H, d,  $J=9$  Hz), 8.69 (1H, s), 8.19 (2H, m), 7.93 (1H, d,  $J=2$  Hz), 7.67 (1H, t,  $J=8$  Hz), 7.58 (1H, dd,  $J=9$  Hz / 2 Hz), 7.54 (1H, s).

**6-(6-Amino-pyrimidin-4-yloxy)-naphthalene-1-carboxylic acid (8)**: Sodium azide (8.65 g; 133 mmol) was added to a solution of **7** (20.0 g; 66.5 mmol) in DMF (220 mL). The mixture was stirred for 100 min at 65 °C giving 6-(6-azido-pyrimidin-4-yloxy)-naphthalene-1-carboxylic acid. Pd/C 10 % (4 g) was added to the cooled reaction mixture, which was then hydrogenated at normal pressure. The catalyst was filtered off and the filtrate partially evaporated. Pouring the residue into water (2 L) and aq. citric acid (10 %; 60 mL) led to crystallization. Compound **8** was filtered off and washed with water (10.7 g; 57 %): MS:  $[M+1]^+ = 282$ ;  $^1\text{H-NMR}$  (DMSO- $d_6$ );  $\delta$  [ppm]: 13.2 (1H, sb), 8.94 (1H, d,  $J=9$  Hz), 8.15 (3H, m), 7.82 (1H, d,  $J=2$  Hz), 7.64 (1H, t,  $J=8$  Hz), 7.49 (1H, dd,  $J=9$  Hz / 2 Hz), 6.90 (2H, sb), 5.82 (1H, s).

**6-(6-Amino-pyrimidin-4-yloxy)-naphthalene-1-carboxylic acid (3-trifluoromethyl-phenyl)-amide (9)**:

Compound **9** was prepared analogously to **4** (700 mg; 64 %): mp: 243-245 °C; MS:  $[M+1]^+ = 425$ ;  $^1\text{H-NMR}$  (DMSO- $d_6$ );  $\delta$  [ppm]: 10.96 (1H, s), 8.35 (1H, s), 8.29 (1H, d,  $J=9$  Hz), 8.12 (2H, m), 8.04 (1H, d,  $J=8$  Hz), 7.83 (2H, m), 7.67 (2H, m), 7.51 (1H, d,  $J=8$  Hz), 7.45 (1H, d,  $J=9$  Hz), 6.91 (2H, s), 5.84 (1H, s).

**6-(6-Amino-pyrimidin-4-yloxy)-naphthalene-1-carboxylic acid (4-fluoro-3-trifluoromethyl-phenyl)-amide**

**(10)**: Compound **10** was prepared analogously to **4** (2.47 g; 70 %): mp: 223 °C; MS:  $[M+1]^+ = 443$ ;  $^1\text{H-NMR}$  (DMSO- $d_6$ );  $\delta$  [ppm]: 10.97 (1H, s), 8.37 (1H, m), 8.29 (1H, d,  $J=9$  Hz), 8.11 (3H, m), 7.83 (2H, m), 7.68 (1H, t,  $J=8$  Hz), 7.58 (1H, t,  $J=10$  Hz), 7.45 (1H, dd,  $J=9$  Hz / 2 Hz), 6.91 (2H, s), 5.84 (1H, s).

**6-(6-Amino-pyrimidin-4-yloxy)-naphthalene-1-carboxylic acid (3-ethyl-phenyl)-amide (11)**: Compound **11**

was prepared analogously to **4** (135 mg; 56 %): mp: 251-252 °C; MS:  $[M+1]^+ = 385$ ;  $^1\text{H-NMR}$  (DMSO- $d_6$ );  $\delta$  [ppm]: 10.56 (1H, s), 8.26 (1H, d,  $J=9$  Hz), 8.11 (1H, s), 8.08 (1H, d,  $J=8$  Hz), 7.81 (1H, d,  $J=2$  Hz), 7.75 (1H, d,  $J=7$  Hz), 7.72 (1H, s), 7.65 (2H, m), 7.44 (1H, dd,  $J=9$  Hz / 2 Hz), 7.30 (1H, t,  $J=8$  Hz), 7.00 (1H, d,  $J=8$  Hz), 6.91 (2H, s), 5.82 (1H, s), 2.64 (2H, q,  $J=8$  Hz), 1.22 (3H, t,  $J=8$  Hz).

40

**6-(6-Chloro-pyrimidin-4-yloxy)-naphthalene-1-carboxylic acid (3-trifluoromethyl-phenyl)-amide (12):**

Compound **12** was prepared analogously to **4** (13.6 g; 92 %): MS:  $[M+1]^+ = 444$ ;  $^1\text{H-NMR}$  ( $\text{CDCl}_3\text{-d}$ );  $\delta$  [ppm]: 8.61 (1H, s), 8.52 (1H, d,  $J=9$  Hz), 8.04 (1H, s), 8.01 (1H, d,  $J=9$  Hz), 7.93 (2H, m), 7.80 (1H, d,  $J=7$  Hz), 7.72 (1H, d,  $J=2$ ), 7.58 (2H, m), 7.49 (1H, d,  $J=8$ ), 7.42 (1H, dd,  $J=9$  Hz / 3 Hz), 7.05 (1H, s).

**6-[5-(3-Trifluoromethyl-phenylcarbamoyl)-naphthalen-2-yloxy]-pyrimidine-4-carboxylic acid ethyl ester**

**(13)**: A mixture of **12** (11.2 g; 25.2 mmol),  $\text{Et}_3\text{N}$  (7.0 mL; 50.5 mmol) and  $\text{PdCl}_2[\text{P}(\text{C}_6\text{H}_5)_3]_2$  (1.785 g; 2.52 mmol) in EtOH (150 mL) was prepared under a CO-atmosphere of 120 bar in an autoclave and then heated for 30 h at 110 °C. After cooling to rt, the mixture was diluted with EtOH and filtered. The residue was washed thoroughly with EtOH and the filtrate concentrated. Column chromatography ( $\text{SiO}_2$ ;  $\text{CH}_2\text{Cl}_2/\text{EtOAc}$  19:1  $\rightarrow$  9:1), partial concentration and filtration led to the **13** (9.5 g; 78 %): MS:  $[M+1]^+ = 482$ ;  $^1\text{H-NMR}$  ( $\text{CDCl}_3\text{-d}$ );  $\delta$  [ppm]: 8.91 (1H, s), 8.52 (1H, d,  $J=9$  Hz), 8.05 (1H, s), 8.01 (1H, d,  $J=9$  Hz), 7.9 (2H, m), 7.80 (1H, d,  $J=8$  Hz), 7.74 (1H, d,  $J=2$ ), 7.71 (1H, s), 7.6 (2H, m), 7.49 (1H, d,  $J=8$ ), 7.43 (1H, dd,  $J=9$  Hz / 2 Hz), 4.54 (2H, q,  $J=7$  Hz), 1.50 (3H, t,  $J=7$  Hz).

**6-(6-Hydroxymethyl-pyrimidin-4-yloxy)-naphthalene-1-carboxylic acid (3-trifluoromethyl-phenyl)-amide**

**(BFH772)**:  $\text{NaBH}_4$  (24 mg; 0.6 mmol) was added to a suspension of **13** (241 mg; 0.50 mmol) in *t*-butanol (7 mL). The mixture was stirred for 30 min at 65 °C and then diluted with EtOAc and a saturated aq. solution of  $\text{NaHCO}_3$ . The aq. layer was separated off and re-extracted with EtOAc (2x). The org. layers were washed with a saturated aq. solution of  $\text{NaHCO}_3$  and brine, dried ( $\text{Na}_2\text{SO}_4$ ) and concentrated. Column chromatography ( $\text{SiO}_2$ ;  $\text{CH}_2\text{Cl}_2/\text{EtOAc}$  65:35  $\rightarrow$  1:1) led to BFH772 (133 mg; 61 %): mp: 183-184 °C; MS:  $[M+1]^+ = 440$ ;  $^1\text{H-NMR}$  ( $\text{DMSO-d}_6$ );  $\delta$  [ppm]: 10.98 (1H, s), 8.68 (1H, s), 8.35 (1H, s), 8.32 (1H, d,  $J=9$  Hz), 8.13 (1H, d,  $J=8$  Hz), 8.04 (1H, d,  $J=9$  Hz), 7.93 (1H, d,  $J=2$  Hz), 7.85 (1H, d,  $J=7$  Hz), 7.70 (1H, t,  $J=8$  Hz), 7.65 (1H, t,  $J=8$  Hz), 7.52 (1H, m), 7.50 (1H, d,  $J=2$  Hz), 7.13 (1H, s), 5.70 (1H, t,  $J=6$  Hz), 4.57 (2H, d,  $J=6$  Hz).

**6-(6-Cyano-pyrimidin-4-yloxy)-naphthalene-1-carboxylic acid (3-trifluoromethyl-phenyl)-amide (14):**

DABCO (0.42 g; 3.74 mmol) and KCN (1.0 g; 15.34 mmol) were added to a solution of **12** (3.32 g; 7.48 mmol)

41

1  
2 in DMSO (100 mL) and water (20 mL). The mixture was stirred for 30 min at 55 °C and then poured into water  
3  
4 (1.2 L). This aq. mixture was extracted with EtOAc (3x). The org. layers were washed with water and brine,  
5  
6 dried (Na<sub>2</sub>SO<sub>4</sub>) and concentrated. Column chromatography (SiO<sub>2</sub>; CH<sub>2</sub>Cl<sub>2</sub>/EtOAc 98:2 → 93:7), partial  
7  
8 concentration, dilution with hexane and filtration led to **14** (1.27 g; 39 %): mp: 167 °C; MS: [M+1]<sup>+</sup> = 435; <sup>1</sup>H-  
9  
10 NMR (CDCl<sub>3</sub>-d); δ [ppm]: 8.87 (1H, s), 8.56 (1H, d, *J*=9 Hz), 8.04 (1H, s), 8.03 (1H, d, *J*=9 Hz), 7.94 (1H, d,  
11  
12 *J*=8 Hz), 7.87 (1H, s), 7.84 (1H, d, *J*=8 Hz), 7.74 (1H, d, *J*=2), 7.63 (1H, t, *J*=8), 7.58 (1H, t, *J*=8 Hz), 7.50 (1H,  
13  
14 d, *J*=7 Hz), 7.42 (2H, m).  
15  
16  
17  
18  
19  
20  
21  
22

## 23 Notes

24  
25  
26  
27 The authors declare no competing financial interest.  
28  
29  
30  
31  
32

## 33 References

- 34  
35  
36  
37 (1) Carmeliet, P. Angiogenesis in health and disease. *Nat. Med.* **2003**, *9*, 653-660.  
38  
39  
40 (2) (a) Plate, K.H.; Breier, G.; Weich, H.A.; Risau W. Vascular endothelial growth factor is a potential tumour  
41  
42 angiogenesis factor in human gliomas *in vivo*. *Nature* **1992**, *359*, 845-848. (b) Senger, D.R.; Van de Water, L.;  
43  
44 Brown, L.F.; Nagy, J.A.; Yeo, K.T.; Yeo, T.K.; Berse, B.; Jackman, R.W.; Dvorak, A.M.; Dvorak, H.F.  
45  
46 Vascular permeability factor (VPF, VEGF) in tumor biology. *Cancer Metastasis Rev.* **1993**, *12*, 303-324. (c)  
47  
48 Carmeliet, P.; Ferreira, V.; Breier, G.; Pollefeyt, S.; Kieckens, L.; Gertsenstein, M.; Fahrig, M.; Vandenhoeck,  
49  
50 A.; Harpal, K.; Eberhardt, C.; Declercq, C.; Pawling, J.; Moons, L.; Collen, D.; Risau, W.; Nagy, A. Abnormal  
51  
52 blood vessel development and lethality in embryos lacking a single VEGF allele. *Nature* **1996**, *380*, 435-439.  
53  
54 (d) Klagsbrun, M.; D'Amore, P.A. Vascular endothelial growth factor and its receptors. *Cytokine Growth*  
55  
56  
57  
58  
59  
60 *Factor Rev.* **1996**, *7*, 259-270.

42

- 1  
2  
3 (3) Folkman, J. Angiogenesis in cancer, vascular, rheumatoid and other disease. *Nat. Med.* **1995**, *1*, 27-31.  
4  
5 (4) (a) Folkman, J. Tumor angiogenesis. *Adv. Cancer Res.* **1985**, *43*, 175-203. (b) Folkman, J. The role of  
6  
7 angiogenesis in tumor growth. *Semin. Cancer Biol.* **1992**, *3*, 65-71. (c) Plate, K.H.; Breier, G.; Risau, W.  
8  
9 Molecular mechanisms of developmental and tumor angiogenesis. *Brain Pathol.* **1994**, *4*, 207-218.  
10  
11 (5) Martiny-Baron, G.; Marmé, D. VEGF-mediated tumour angiogenesis: a new target for cancer therapy. *Curr.*  
12  
13 *Opin. Biotechnol.* **1995**, *6*, 675-680.  
14  
15 (6) (a) Liotta, L.A.; Steeg, P.S.; Stetler-Stevenson, W.G. Cancer metastasis and angiogenesis: an imbalance of  
16  
17 positive and negative regulation. *Cell* **1991**, *64*, 327-336. (b) Parangi, S.; O'Reilly, M.; Christofori, G.;  
18  
19 Holmgren, L.; Grosfeld, J.; Folkman, J.; Hanahan, D. Antiangiogenic therapy of transgenic mice impairs de  
20  
21 novo tumor growth. *Proc. Natl. Acad. Sci.* **1996**, *93*, 2002-2007.  
22  
23 (7) Folkman, J. Anti-angiogenesis: new concept for therapy of solid tumors. *Ann. Surgery* **1972**, *175*, 409-416.  
24  
25 (8) (a) Sitohy, B.; Nagy, J.A.; Dvorak, H.F. Anti-VEGF/VEGFR therapy for cancer: reassessing the target.  
26  
27 *Cancer Res.* **2012**, *72*, 1909-1914. (b) Musumeci, F.; Radi, M.; Brullo, C.; Schenone, S. Vascular endothelial  
28  
29 growth factor (VEGF) receptors: drugs and new inhibitors. *J. Med. Chem.* **2012**, *55*, 10797-10822. (c) Zhang,  
30  
31 C.; Tan, C.; Ding, H.; Xin, T.; Jiang, Y. Selective VEGFR inhibitors for anticancer therapeutics in clinical use  
32  
33 and clinical trials. *Curr. Pharmaceut. Design* **2012**, *18*, 2921-2935.  
34  
35 (9) Bold, G.; Altmann, K.H.; Frei, J.; Lang, M.; Manley, P.W.; Traxler, P.; Wietfeld, B.; Brüggén, J.;  
36  
37 Buchdunger, E.; Cozens, R.; Ferrari, S.; Furet, P.; Hofmann, F.; Martiny-Baron, G.; Mestan, J.; Rösel, J.; Sills,  
38  
39 M.; Stover, D.; Acemoglu, F.; Boss, E.; Emmenegger, R.; Lässer, R.; Masso, E.; Roth, R.; Schlachter, C.;  
40  
41 Vetterli, W. New anilinophthalazines as potent and orally well absorbed inhibitors of the VEGF receptor  
42  
43 tyrosine kinases useful as antagonists of tumor-driven angiogenesis. *J. Med. Chem.* **2000**, *43*, 2310-2323. *ibid.*  
44  
45 **2000**, *43*, 3200.  
46  
47  
48  
49  
50  
51  
52  
53  
54  
55  
56  
57  
58  
59  
60

43

(10) Manley, P.W.; Furet, P.; Bold, G.; Brügggen, J.; Mestan, J.; Meyer, T.; Schnell, C.; Wood, J.; Haberey, M.; Huth, A.; Krüger, M.; Menrad, A.; Ottow, E.; Seidelmann, D.; Siemeister, G.; Thierauch K.H. Anthranilic acid amides: a novel class of antiangiogenic VEGF receptor kinase inhibitors. *J. Med. Chem.* **2002**, *45*, 5687-5693.

(11) Two independent patent applications were published describing BAW2881 as an example: (a) Potashman, M.; Kim, T.; Bellon, S.; Booker, S.; Cheng, Y.; Kim, J.L.; Tasker, A.; Xi, N.; Xu, S.; Harmange, J.C.; Borg, G.; Weiss, M.; Hodous, B.L.; Graceffa, R.; Buckner, W.H.; Masse, C.E.; Choquette, D.; Martin, M.W.; Germain, J.; Dipietro, L.V.; Chaffee, S.C.; Nunes, J.J.; Buchanan, J.L.; Habgood, G.J.; McGowan, D.C.; Whittington, D.A.; **2005**. Compounds and methods of use. WO 2005 / 070891. (b) Bold, G.; Capraro, H.G.; Caravatti, G.; Flörsheimer, A.; Furet, P.; Manley, P.W.; Vaupel, A.; Pissot-Soldermann, C.; Gessier, F.; Schnell, C.; Littlewood-Evans, A.J.; Kapa, P.K.; Bajwa, J.S.; Jiang, X.; **2006**. Bicyclic amides as kinase inhibitors. WO 2006 / 059234. Biological activities of two of the compounds were described in: (c) Halin, C.; Fahrngruber, H.; Meingassner, J.G.; Bold, G.; Littlewood-Evans, A.; Stütz, A.; Detmar, M. Inhibition of chronic and acute skin inflammation by treatment with a vascular endothelial growth factor receptor tyrosine kinase inhibitor. *Am. J. Pathology* **2008**, *173*, 265-277. (d) Meingassner, J.G.; Fahrngruber, H.; Kowalsky, E.; Billich, A.; Bold, G.; Littlewood-Evans, A.; Stütz, A. NVP-BFH772, a potent inhibitor of VEGF receptor tyrosine kinases, is effective in models of skin inflammation. *J. Investig. Derm.* **2011**, *131*, Supplement Abstr. 480.

(12) Shieh, W.C.; McKenna, J.; Sclafani, J.A.; Xue, S.; Girgis, M.; Vivello, J.; Radetich, B.; Prasad, K. Syntheses of a triad of Flt3 kinase inhibitors: from bench to pilot plant. *Org. Process Res. & Develop.* **2008**, *12*, 1146-1155.

(13) Weissberg, E.; Rösel, J.; Bold, G.; Furet, P.; Jiang, J.; Cools, J.; Wright, R.D.; Nelson, E.; Barrett, R.; Ray, A.; Moreno, D.; Hall-Meyers, E.; Stone, R.; Galinsky, I.; Fox, E.; Gilliland, G.; Daley, J.F.; Lazo-Kallanian, S.; Kung, A.L.; Griffin, J.D. Antileukemic effects of the novel, mutant FLT3 inhibitor NVP-AST487: effects on PKC412-sensitive and -resistant FLT3-expressing cells. *Blood* **2008**, *112*, 5161-5170.

(14) Akeno-Stuart, N.; Croyle, M.; Knauf, J.A.; Malaguarnera, R.; Vitagliano, D.; Santoro, M.; Stephan, C.; Grosios, K.; Wartmann, M.; Cozens, R.; Caravatti, G.; Fabbro, D.; Lane H.A.; Fagin, J.A. The RET kinase

44

1  
2 inhibitor NVP-AST487 blocks growth and calcitonin gene expression through distinct mechanisms in medullary  
3 thyroid cancer cells. *Cancer Res.* **2007**, *67*, 6956-6964.

4  
5  
6  
7 (15) Wood, J.M.; Bold, G.; Buchdunger, E.; Cozens, R.; Ferrari, S.; Frei, J.; Hofmann, F.; Mestan, J.; Mett, H.;  
8 O'Reilly, T.; Persohn, E.; Rösel, J.; Schnell, C.; Stover, D.; Theuer, A.; Towbin, H.; Wenger, F.; Woods-Cook,  
9 K.; Menrad, A.; Siemeister, G.; Schirner, M.; Thierauch, K.H.; Schneider, M.R.; Drevs, J.; Martiny-Baron, G.;  
10 Totzke, F.; Marmé, D. PTK787/ZK 222584, a novel and potent inhibitor of vascular endothelial growth factor  
11 receptor tyrosine kinases, impairs vascular endothelial growth factor-induced responses and tumor growth after  
12 oral administration. *Cancer Res.* **2000**, *60*, 2178-2189.

13  
14  
15  
16 (16) Manley, P.W.; Bold, G.; Brügggen, J.; Fendrich, G.; Furet, P.; Mestan, J.; Schnell, C.; Stolz, B.; Meyer, T.;  
17 Meyhack, B.; Stark, W.; Strauss, A.; Wood, J.. Advances in the structural biology, design and clinical  
18 development of VEGF-R kinase inhibitors for the treatment of angiogenesis. *Biochimica et Biophysica Acta*,  
19 *Proteins and Proteomics* **2004**, *1697*, 17-27.

20  
21  
22 (17) At the time this work was accomplished, there was no crystal structure of the FLT3 kinase in the “DFG out”  
23 conformation available. We resorted to a homology model described in: Weisberg, E.; Rösel, J.; Furet, P.; Bold,  
24 G.; Imbach, P.; Flörsheimer, A.; Caravatti, G.; Jiang, J.; Manley, P.W.; Ray, A.; Griffin, J.D. Antileukemic  
25 effects of novel first-and second-generation FLT3 inhibitors: structure-affinity comparison. *Genes & Cancer*  
26 **2010**, *1*, 1021-1032.

27  
28  
29 (18) Warmuth, M.; Kim, S.; Gu, X.J.; Xia, G.; Adrián, F. Ba/F3 cells and their use in kinase drug discovery.  
30 *Curr. Opin. Oncol.* **2007**, *19*, 55-60.

31  
32 (19) Buchdunger, E.; Trinks, U.; Mett, H.; Regenass, U.; Müller, M.; Meyer, T.; McGlynn, E.; Pinna, L.A.;  
33 Traxler, P.; Lydon, N.B. 4,5-Dianilinophthalimide: a protein-tyrosine kinase inhibitor with selectivity for the  
34 epidermal growth factor receptor signal transduction pathway and potent *in vivo* antitumor activity. *Proc Natl*  
35 *Acad Sci USA* **1994**, *91*, 2334-2338.

45

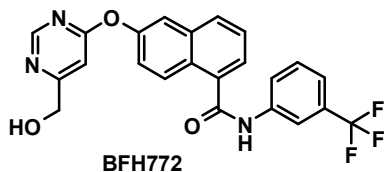
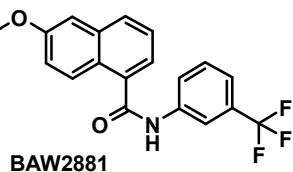
- (20) LaMontagne, K.; Littlewood-Evans, A.; Schnell, C.; O'Reilly, T.; Wyder, L.; Sanchez, T.; Probst, B.; Butler, J.; Wood, A.; Liao, G.; Billy, E.; Theuer, A.; Hla, T.; Wood, J. Antagonism of sphingosine-1-phosphate receptors by FTY720 inhibits angiogenesis and tumor vascularization. *Cancer Res.* **2006**, *66*, 221-231.
- (21) Weidensteiner, C.; Rausch, M.; McSheehy, P.M. J.; Allegrini, P.R. Quantitative dynamic contrast-enhanced MRI in tumor-bearing rats and mice with inversion recovery TrueFISP and two contrast agents at 4.7 T. *Journal of Magnetic Resonance Imaging* **2006**, *24*, 646–656.
- (22) Moss, A. The angiotensin II type 2 interaction: a potential target for future therapies in human vascular disease. *Cytokine Growth Factor Rev.* **2013**, *24*, 579-592.
- (23) Fallahi, P.; Mazzi, V.; Vita, R.; Ferrari, S.M.; Materazzi, G.; Galleri, D.; Benvenga, S.; Miccoli, P.; Antonelli, A. New therapies for dedifferentiated papillary thyroid cancer. *Int. J. Mol. Sci.* **2015**, *16*, 6153-6182.
- (24) Ravegnini, G.; Nannini, M.; Sammarini, G.; Astolfi, A.; Biasco, G.; Pantaleo, M.A.; Hrelia, P.; Angelini, S. Personalized medicine in gastrointestinal stromal tumor (GIST): Clinical implications of the somatic and germline DNA analysis. *Int. J. Mol. Sci.* **2015**, *16*, 15592-15608.
- (25) (a) Fallahi, P.; Ferrari, S.M.; Antonelli, A.; Di Bari, F.; Benvenga, S.; Spisni, R.; Materazzi, G.; Miccoli, P. Selective use of vandetanib in the treatment of thyroid cancer. *Drug Des. Devel. Ther.* **2015**, *9*, 3459-3470. (b) Lacouture, M.E.; Wu, S.; Robert, C.; Atkins, M.B.; Kong, H.H.; Guitart, J.; Garbe, C.; Hauschild, A.; Puzanov, I.; Alexandrescu, D.T.; Anderson, R.T.; Wood, L.; Dutcher, J.P. Evolving strategies for the management of hand-foot skin reaction associated with the multitargeted kinase inhibitors sorafenib and sunitinib, *Oncologist* **2008**, *13*, 1001-1011.
- (26) Ellis, L.M.; Hicklin, D.J. Pathways mediating resistance to vascular endothelial growth factor-targeted therapy. *Clin Cancer Res.* **2008**, *14*, 6371-6375.
- (27) Ding, C.; Zhang, C.; Zhang, M.; Chen, Y.Z.; Tan, C.; Tan, Y.; Jiang, Y. Multitarget inhibitors derived from crosstalk mechanism involving VEGFR2. *Future Med. Chem.* **2014**, *6*, 1771-1789.

46

1  
2  
3 (28) Boulay, A.; Breuleux, M.; Stephan, C.; Fux, C.; Brisken, C.; Fiche, M.; Wartmann, M.; Stumm, M.; Lane,  
4  
5 H.A.; Hynes, N.E. The Ret receptor tyrosine kinase pathway functionally interacts with the ER $\alpha$  pathway in  
6  
7 breast cancer. *Cancer Res.* **2008**, *68*, 3743-3751.  
8

9  
10 (29) Ferretti, S.; Allegrini, P.R.; O'Reilly, T.; Schnell, C.; Stumm, M.; Wartmann, M.; Wood, J.; McSheehy,  
11  
12 P.M. Patupilone induced vascular disruption in orthotopic rodent tumor models detected by magnetic resonance  
13  
14 imaging and interstitial fluid pressure. *Clin. Cancer Res.* **2005**, *11*, 7773-7784.  
15  
16  
17  
18  
19  
20  
21  
22  
23  
24  
25  
26  
27  
28  
29  
30  
31  
32  
33  
34  
35  
36  
37  
38  
39  
40  
41  
42  
43  
44  
45  
46  
47  
48  
49  
50  
51  
52  
53  
54  
55  
56  
57  
58  
59  
60

## Table of Contents Graphic

1  
2  
3  
4  
5  
6  
7  
8  
9  
10  
11  
12  
13  
14  
15  
16  
17  
18  
19  
20  
21  
22  
23  
24  
25  
26  
27  
28  
29  
30  
31  
32  
33  
34  
35  
36  
37  
38  
39  
40  
41  
42  
43  
44  
45  
46  
47  
48  
49  
50  
51  
52  
53  
54  
55  
56  
57  
58  
59  
60

cpd	dose [mg/kg]	prim. tumor T/C	metastasis T/C
PTK787	100	0.44	0.34
BAW2881	3	0.46	0.29
BFH772	3	0.36	0.17

Potency and efficiency in an orthotopic B16 melanoma model. Primary tumor and metastatic growth inhibition expressed by T/C (treated over control).